AE 4723 – Aircraft Dynamics & Control
Interim Report 2

I/we, Tyler Guertin and

John Spencer Kerwin and

Martin Runquist submit the AE 4723 Project Report.

Our signature(s) below affirm(s) that all of the writing in this submission is my/our original work. Any reference material that I/we used to prepare this submission, including text or video resources, but excluding the lecture notes provided on the Canvas site for this course, is properly cited.

Statement of team member contributions (check one box)

☐ Not applicable: I worked alone.

X Each group member contributed equally to this submission.

☐ The contributions of each group member are as follows:

Student	**Contribution (%)**

We have read and understand WPI's Academic Honesty Policy, and our conduct in preparing this submission has been in accordance with this Policy.

Signatures (all group members must sign):

Tyler Guertin John Spencer Kerwin Martin Runquist

1 Aircraft Description

The commercial airline industry is an important part of modern aviation, with the majority of publicly known aircraft lying in this sector. An abundance of information is available on commercial airliners due to the stringency of regulations for passenger aircraft. For this reason, the Boeing 747-400 was chosen. The 747 was introduced in the mid 1960's and has been a staple of modern long-haul transportation for 52 years. We were interested in the 747 because of its incredibly long service record and how an aircraft designed half a century ago remains relevant today.

Table 1: Boeing 747-400 Basic Data

Data Point	Value
Weight	3556 KN
Cruise Altitude	6 km
Cruise Speed	258.2 m/s
Wing Surface Area	541.2 m^2
Wingspan	64.44 m
Propulsion	4 x 252400 N Pratt & Whitney PW-4056 turbofans
Tail span	22.17 m
Tail area	136.57 m^2
Tail mean chord	6.16 m
$\overline{V}_H$	0.81

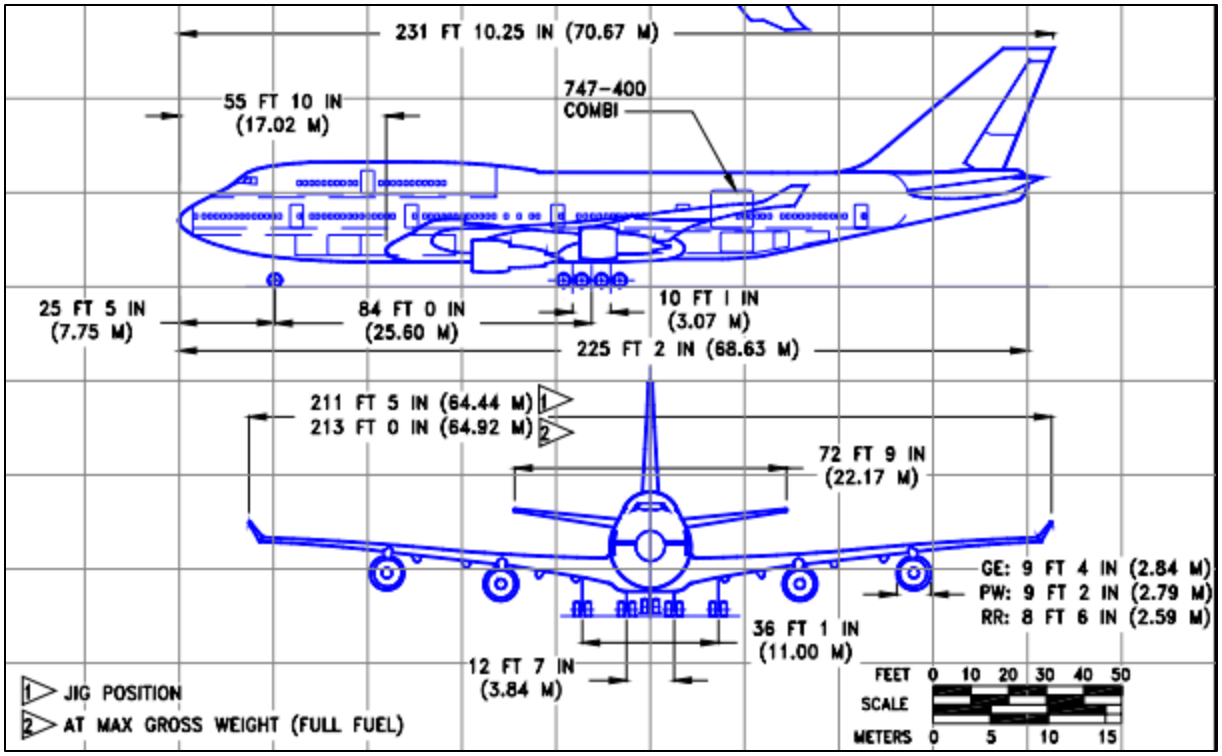

Figure 1: Technical Diagram of Boeing 747-400

2 Performance Characteristics

Performance Analysis is a critical part of determining parameters for safe operation of aircraft. All parameters found below are characteristic ceilings and limits that affect the performance of the aircraft, and how its dynamics can be modeled. Cruise conditions were set at 6 km and a velocity of 0.85 Mach or 258.2 m/s at the given altitude, according to the standard atmosphere model and the definition of published specifications of the aircraft.

2.1 Thrust required at cruise conditions and Lift to Drag curve

The maximum thrust for a typical Boeing 747 is 1.01 MN at sea level. For a realistic value of thrust at the cruise trim condition stated above, the thrust would have to be below this limit. Equation 1 characterizes the relationship between W and the lift-drag ratio to calculate the thrust required at trim conditions with no rate of climb.

$$T = \frac{W}{\left(\frac{L}{D}\right)} \tag{1}$$

This directly depends on the weight of the aircraft, as well as the lift-drag ratio at the given velocity and altitude. The thrust required is 270.5 kN, which seems relatively low, but considering that maximum thrust is generally achieved at takeoff, cruise speed requires much less thrust in comparison.

2.2 Glide Range

The glide range of an aircraft is the theoretical distance that an aircraft can travel from a given altitude with no engine thrust, with only the control of aerodynamic surfaces. This is a function of the height of the aircraft as well as the lift to drag ratio. Understanding the glide range of an aircraft is important to prepare contingencies for unexpected loss of thrust during flight.

Glide range was examined in two separate conditions for the 747. The first of which was seen to be the absolute glide range, which is the glide range from 13.39 km which was calculated to be the service ceiling. This glide range provides the theoretical absolute maximum glide range from the service ceiling to sea level, h = 0 km. A 747 at 13.39 km has an expected glide range with thrust equal to zero of 225 km. The second condition that was examined was the glide range from the perspective of an aircraft at a typical cruise altitude of 6 km. If it is presumed that the aircraft is unable to produce thrust at this altitude, then by Equation 2 the glide range to h = 0 km would be 100.5 km. Glide range is a function of the drag to lift ratio and height of the aircraft, since thrust will be completely reduced to zero in any glide condition.

$$\boldsymbol{Glide\ Range} = \frac{\boldsymbol{h}}{\left(\frac{\boldsymbol{C_d}}{\boldsymbol{C_L}}\right)} \quad \textbf{(2)}$$

2.3 Absolute and Service Ceilings

The two datapoints that demonstrate the altitude at which an aircraft can operate are the absolute and service ceilings. The absolute ceiling is the altitude at which the aircraft cannot climb any higher, or has a maximum rate of climb (RC_{max}) of zero. At a lower altitude, the service ceiling can be found, determined by the point at which the aircraft can achieve a maximum rate of climb of 100 feet per minute. Aircraft typically do not fly above the service ceiling, as the climb rate of 100 feet per minute provides a buffer to allow for maneuvers as needed. Flying at the absolute ceiling is inadvisable as the aircraft will be physically unable to increase its altitude in the case of an emergency and may have poor performance characteristics.

As noted above, the typical cruise condition of the 747 was set to be 6 km. This is a typical cruise height far below the service and absolute ceiling of 13 km that can be attained by the aircraft (Modern Airliners, 2022). The calculated service ceiling of 13.39 km is within a reasonable range of the service ceiling of 13 km published by modernairliners.net.

For the 747, the service ceiling is 13.39 km, with the absolute ceiling being slightly higher at 13.61 km. Between the service ceiling and absolute ceiling flight can be unstable, but for all intents and purposes the absolute ceiling is where the aircraft is physically unable to generate climb above zero.

Service Ceiling ~13.39 km
Absolute Ceiling ~ 13.61 km

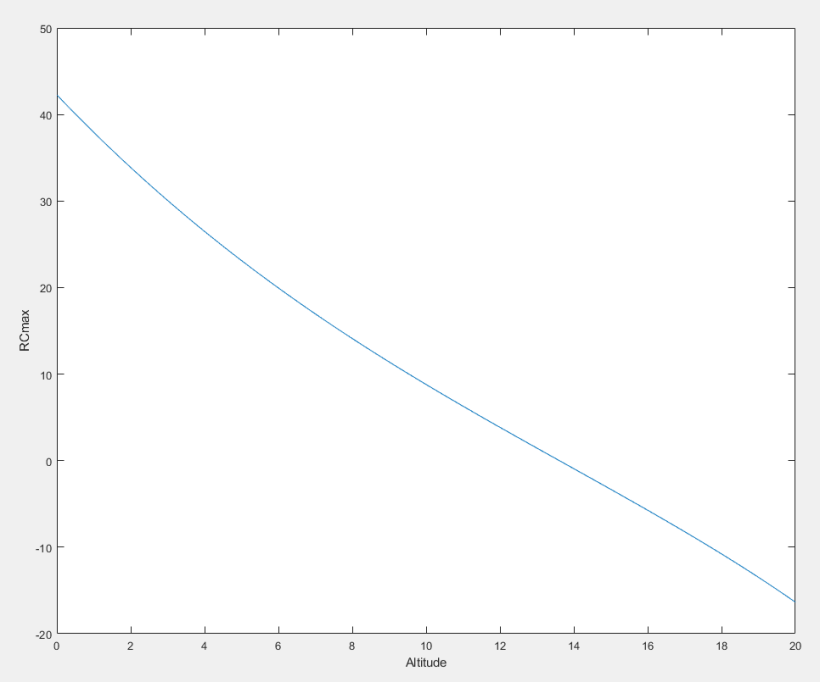

Figure 2: RCmax vs Altitude

The absolute and service ceilings were extrapolated graphically in Figure 2 at the points where velocity was comparable to the critical points mentioned above. This figure compares the RC_{max} values at different given altitudes. Unfortunately, this model is based on a standard atmospheric model that provides reliable results up to an altitude of 11 km. Although the calculated values are reasonable, they are not valid for proper aircraft analysis as the aircraft performance model will be inaccurate.

2.4 Minimum Radius of Turn

The minimum radius of turn of an aircraft is a measure of how tightly an aircraft can turn in a horizontal plane under particular conditions. Because many factors can affect this, a single radius of turn only provides information for the condition it describes.

Determining the minimum radius of turn requires first calculating the various load factors of thrust, angle of attack, and structure ($n_{max,t}$, $n_{max,\alpha}$, $n_{max,s}$); Equations 4-6 describe expressions for these load factors.. Because information about the structural load factor is rarely the limiting factor, and is not readily published, this calculation was omitted in our process. The angle of attack load factor also depends on calculating the angle of attack induced load, calculating the angle of attack induced load, $L_{max,\alpha}$, outlined in Equation 3. If any of the three load factors is exceeded during a turn, the aircraft will fail, thus the minimum load factor is used in the calculation of the minimum turn radius (Eqn 7).

$$\boldsymbol{L_{max,\,\alpha} = \frac{1}{2}\rho V^2 s C_{Lmax}} \qquad \textbf{(3)}$$

$$n_{max,t} = \sqrt{\frac{Q}{K\left(\frac{W}{S}\right)}\left(\frac{T_{max}}{W} - \frac{QC_{Do}}{\left(\frac{W}{S}\right)}\right)} \quad (4)$$

$$n_{max,\alpha} = \frac{L_{max,\alpha}}{W} \quad (5)$$

$$n_{max,s} = \frac{L_{max,s}}{W} \quad (6)$$

$$n_{max} = \min\{n_{max,s};\ n_{max,\alpha};\ n_{max,t}\} \quad (7)$$

$$R_{min} = \frac{V^2}{g\sqrt{n_{max}^2 - 1}} \quad (8)$$

After the minimum load factor is determined, it can be used to determine the minimum turn radius for a given airspeed, as shown in Equation 8.

No reputable source for C_{Lmax} data was found. An unknown experiment/simulation conducted by Virginia Tech claims a C_{Lmax} at sea level of 1.85 (Virginia Tech, 1993). For the purposes of our calculations, we used this value. For C_{Lmax} at cruise altitude, the value from sea level was multiplied by the ratio of the atmospheric density at sea level to the density at cruise altitude. While these values are likely not accurate, they provide a framework to make rough estimate calculations. With this information, the R_{min} at sea level was determined to be 1491 m, while the R_{min} at cruise altitude was determined to be 2075 m. These radii could be feasible, however, in the standard operation of a Boeing 747-400 the radius of any turn would be far greater than the minimum to avoid passenger discomfort or cargo damage.

2.5 Speeds for: Stall, $\left(\frac{L}{D}\right)_{max}$, RC_{max}

For a given altitude there are three airspeeds that are used to describe aircraft performance. Stall speed is defined as the minimum speed an aircraft can maintain level flight. Any speed lower than the stall speed will result in a loss of altitude. The maximum lift-drag ratio speed determines the most efficient speed for an aircraft to travel, maximizing lift while minimizing drag. The maximum rate of climb speed simply defines which airspeed allows for the maximum rate of climb at a given altitude.

Values for the stall speed, maximum lift-drag ratio speed, and maximum rate of climb speed were calculated for the aircraft at sea level and 6 km altitude.

Characteristic Velocity	At Sea Level (m/s)	At Cruise Altitude (6km) (m/s)
Stall	76.15	103.75
$(L/D)_{max}$	131.91	179.71
RC_{max}	238.64	246.74

2.6 Range

As opposed to glide range, range is the distance that an aircraft can travel while powered and traveling at the maximum lift-drag ratio speed. The range of an aircraft is important in determining where it is capable of traveling to and what routes it can take without refueling. In the case of passenger transport, a greater range allows for fewer or no stops between destinations. For this report, range was calculated assuming steady, level flight at cruise altitude, with no takeoff or landing component.

The range of the 747 can be computed using the maximum and minimum aircraft weight, as well as the lift-drag ratio, and the ratio of velocity to the thrust specific fuel consumption. This range assumes fuel consumption flight from full to empty weight. The maximum weight is 3.56 MN and minimum weight of 1.95 MN. The reduction in weight is due to fuel consumption.

$$\boldsymbol{Range} = \left(\frac{\boldsymbol{V}}{\boldsymbol{C_t}}\right)\left(\frac{\boldsymbol{L}}{\boldsymbol{D}}\right)\left(\frac{\boldsymbol{w_0}}{\boldsymbol{w_1}}\right) \quad \textbf{(9)}$$

Fuel Consumption is extrapolated from the thrust at given altitudes, contributing to the thrust specific fuel consumption Ct. The velocity was assumed to be that of the cruise condition. This calculation resulted in a range of 12,689 km using the 4 Pratt & Whitney PW-4056 turbofan engines. This is comparable to published range values.

2.7 Summary of Performance Characteristics

Characteristic	Value
Thrust Required at Cruise	270.5 kN
Glide Range (Service Ceiling, 13.39 km)	225 km
Glide Range (Cruise Altitude, 6km)	100.5 km
Service Ceiling	13.39 km
Absolute Ceiling	13.61 km
Minimum Radius of Turn (Sea Level)	1491 m
Minimum Radius of Turn (Cruise, 6km)	2075 m
Range	12,689 km

3 Trim Calculations and Stability Characteristics

A trim condition of an aircraft is when an aircraft is kept at a set altitude by the aircraft control system with constant control inputs. In a static, no disturbance case, the control input, such as deflection angle and thrust of the engine, is kept constant, with their specific values determine by the condition the aircraft is meant to be set at. The ability of an aircraft to respond to a disturbance and settle to a set condition correlates directly with the aircrafts' stability. The stability of the aircraft is affected by the shape and, more critically, the aerodynamics of the aircraft. The control system can aid the stability by changing the aerodynamics of the aircraft to specific set values, however, the aircraft with set, constant control inputs can have natural stability as well.

3.1 Angle of Attack and Elevator Deflection

The angle of attack and elevator deflection were determined at various altitudes and velocities under a trim condition. At trim condition, the angle of attack and elevator deflection can be related within the definition of the lift coefficient and moment coefficient. The values can be found with defined values of certain lift coefficient derivatives, the weight of the aircraft and altitude and velocity that the trim condition is desired to be at. Equation 10 displays the relations of the coefficients, and the table below describes the angle of attack and elevator deflection at various trim conditions

$$\begin{bmatrix} \alpha_{trim} \\ \delta_{e,trim} \end{bmatrix} = \begin{bmatrix} C_{L_\alpha} & C_{L_{\delta_e}} \\ C_{M_\alpha} & C_{M_{\delta_e}} \end{bmatrix} \begin{bmatrix} \frac{W}{\frac{1}{2}\rho v^2 S} - C_{L_0} \\ -C_{M_0} \end{bmatrix} \tag{10}$$

Angle of Attack and elevator deflection at various trim conditions

	h=0 ft; V=673 ft/s;	**h=20,000 ft; V=673 ft/s;**	**h=40,000 ft; V=673 ft/s;**
α (deg)	13.410	-2.504	4.423
δ_e (deg)	-12.609	1.926	-5.898

3.2 Static Stability

Static stability of an aircraft is the immediate response for the aircraft to move towards equilibrium, as opposed to a long-term, time dependent case. Aircraft are often designed to promote greater static stability to maintain constant control of the aircraft despite any disturbances from the environment. The geometry of the wings, tail, fuselage, and placement of all three are examples of design parameters that affect the stability of an aircraft.

To determine the static longitudinal stability of the 747-400 aircraft the locations of the neutral point and center of gravity were compared. With different configurations and cargo, passenger, and fuel loads, the center of gravity can vary from 10-20% of the chord length (Smart Cockpit). For the purposes of analysis, a center of gravity of 25% of the mean chord was assumed. In addition, no data of the

aerodynamic center of the wing is readily published, so the position of the aerodynamic center was also assumed to be 25% of the mean chord. To calculate the static stability margin, equations 10-12 were used.

$$\boldsymbol{CL,\alpha = CL,\alpha,w + CL,\alpha,t\left(\frac{st}{s}\right)(1 - k\varepsilon,\alpha)} \tag{10}$$

$$\boldsymbol{h_{np} = h_{ac} + \frac{CL,\alpha,t}{CL,\alpha}\overline{V}_H\left(1 - k_{\varepsilon,\alpha}\right)} \tag{11}$$

$$\boldsymbol{Stability\ Percentage\ = 100\left(h_{np}\ -\ h_{ac}\right)} \tag{12}$$

These calculations are all based on the locations of the various points relative to the datum in units of the chord length. A neutral point location of 0.892 was calculated. When compared to the assumed location of the center of gravity at the quarter chord point, the margin of static longitudinal stability was found to be 64.2%. This indicates that the 747-400 is statically stable longitudinally.

3.3 Dynamic Stability at Various Trim Conditions

In contrast to static stability, dynamic stability is the long-term response of an aircraft when placed outside of its equilibrium, often viewed in respect to time and described by the transient response of the aircraft. There are three general categories that define the dynamic stability of an aircraft: unstable, where the aircraft's response to a disturbance moves farther from the equilibrium state as time increases; neutral, where the aircraft oscillates at a constant amplitude away from equilibrium; and stabile, the most important category, where the aircraft's response moves toward the equilibrium state as time increases. Similar to static stability, the aerodynamic characteristics of the aircraft determine the response.

Modes of motion are used to define different types of stable dynamic responses. The two longitudinal modes are phugoid and short period modes, where phugoid modes have slow oscillations, are lightly damped, with motion in Δu and $\Delta\theta$, and short period modes are fast, heavily damped, with motion in Δw, Δq, and $\Delta\alpha$. The three lateral modes are spiral, which is slow, lightly damped, with yaw motion, roll convergence, which is fast, heavily damped, with roll motion, and Dutch roll, which is between the other two in speed and damping and has roll and yaw motion. Each mode correlates to different eigenvalues and the real and imaginary parts relates to the speed of oscillations and damping ratio.

3.4 Modes of Motion; Eigenvalues, Settling Times, Damping Ratios

To determine the eigenvalues and subsequently the modes of motion and settling and damping ratios, published data on the characteristic coefficients of the 747 were found (Koşar et al, 2007; Nelson, 2010). These published values were then used to calculate the appropriate dimensional derivatives which allowed the construction of linearized dynamical models for a

series of Mach numbers and altitudes. These matrices for both longitudinal and lateral stability were constructed as follows in equations 12-15.

$$A_{long} = \begin{bmatrix} \frac{X_u}{m} & \frac{X_w}{m} & 0 & -g\cos\theta^* & 0 \\ \frac{Z_u}{m - Z_{\dot{w}}} & \frac{Z_w}{m - Z_{\dot{w}}} & \frac{Z_q + mu^*}{m - Z_{\dot{w}}} & \frac{-mg\sin\theta^*}{m - Z_{\dot{w}}} & 0 \\ \frac{M_u + M'Z_u}{J_y} & \frac{M_w + M'Z_w}{J_y} & \frac{M_q + M'(Z_q + mu^*)}{J_y} & \frac{-M'mg\sin\theta^*}{J_y} & 0 \\ 0 & 0 & 1 & 0 & 0 \\ -\sin\theta^* & \cos\theta^* & 0 & -u^*\cos\theta^* & 0 \end{bmatrix} \quad (12)$$

$$where\ M' = \frac{M_{\dot{w}}}{m - Z_{\dot{w}}}$$

$$A_{lat} = \begin{bmatrix} Y_v/m & Y_v/m & -V^* + Y_r/m & g\cos\theta^* & 0 & 0 \\ \frac{l_v}{J'_x} + J'_{zx}N_v & \frac{l_p}{J'_x} + J'_{zx}N_p & \frac{l_r}{J'_x} + J'_{zx}N_r & 0 & 0 & 0 \\ \frac{N_v}{J'_z} + J'_{zx}l_v & \frac{N_p}{J'_z} + J'_{zx}l_p & \frac{N_r}{J'_z} + J'_{zx}l_r & 0 & 0 & 0 \\ 0 & 1 & \tan\theta^* & 0 & 0 & 0 \\ 0 & 0 & \sec\theta^* & 0 & 0 & 0 \\ 1 & 0 & 0 & 0 & V^*\cos\theta^* & 0 \end{bmatrix} \quad (13)$$

$$where\ J'_x = \frac{(J_xJ_z - J_{zx}^2)}{J_z}, J'_z = \frac{J_xJ_z - J_{zx}^2}{J_x}, J'_{zx} = J_{zx}(J_xJ_z - J_{zx}^2)$$

After filling out the above matrices with aircraft and state-specific information, the eigenvalues were calculated. Eigenvalues are often calculated with the expression shown in Equation 16. Where A is a known matrix and λ represents an unknown eigenvalue(s). Taking the determinant of the expression on the left side of the equation allows one to solve for λ. This

equation often has multiple solutions, which can include real, imaginary and complex values. The eigenvalues were calculated for the conditions listed in the table below Equation 16.

$$|\boldsymbol{A} - \boldsymbol{\lambda I}| = \mathbf{0} \tag{16}$$

Mach	Altitude	Longitudinal Eig.	Settling Time	Damping Ratios	Lateral Eig.	Settling Time	Dampin g Ratios
0.25	0 ft	-0.3020± 0.6810i	13.2445	0.4054	-1.2535	3.1911	1
		0.0135 ± 0.2143i	Does not settle	0.0629	-0.0504 ± 0.7234i	79.38	0.069
					-0.0486	82.31	1
0.65	20,000 ft	-0.9667 + 3.6493i	4.1377	.2561	Insufficient data		
		-0.0077 + 0.0631i	517.355	.1216			
0.90	40,000 ft	-0.2713 + 1.2810i	14.7462	0.2072	-0.1783 ± 0.9927i	22.4351	0.1768
		-0.0020 + 0.0715i	2024.5	0.0276	-0.4620	8.65	1
					0.0061	Does not settle	N/A

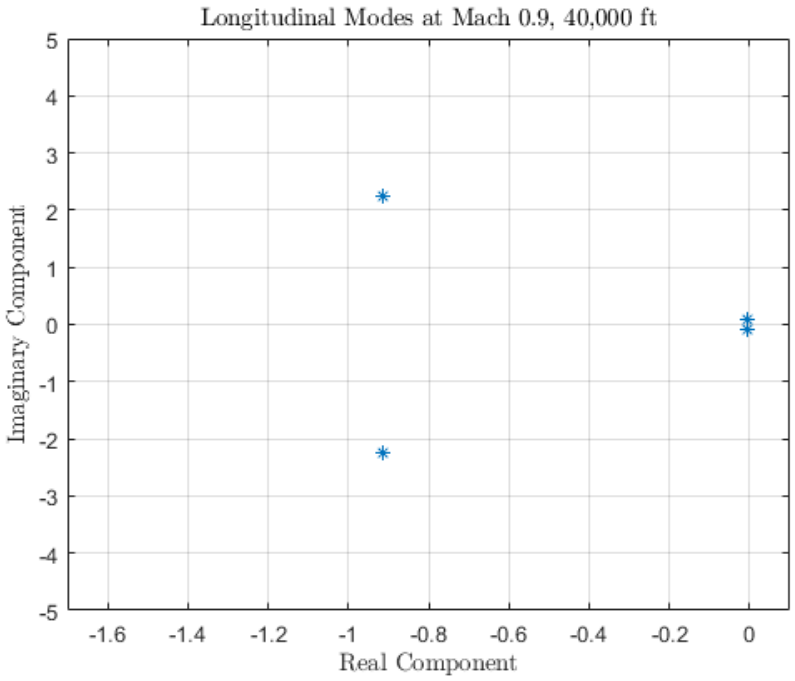

Figure 3: Longitudinal Short Period and Phugoid Modes at Mach 0.9, 40,000 ft

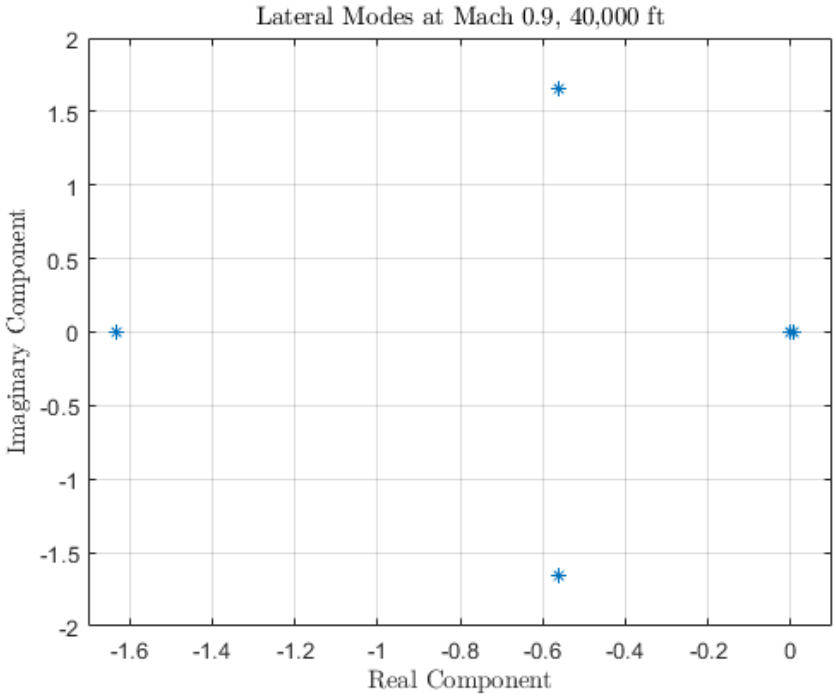

Figure 4: Lateral Roll Convergence, Dutch Roll, and Spiral Modes at Mach 0.9, 40,000 ft

The eigenvalues/modes found for the Boeing 747 fall into the standard types of modes for both longitudinal and lateral stability; specifically, the modes expressed are the phugoid, short-period, roll convergence, Dutch roll, and spiral. All but two modes analyzed contain negative real components, indicating stability. However, two modes have a positive real component: the phugoid mode determined at Mach 0.25 at sea level, and the spiral mode at Mach 0.9 at sea level. Assuming that these positive values are not due to calculation errors, they raise cause for special attention when designing a control system, as the aircraft will not be intrinsically stable in these situations. All phugoid, short-period, and Dutch roll modes contain an imaginary component, indicating oscillatory motion as expected.

4 Control Design and Testing

To design regulation schemes, a Simulink model utilizing a linear quadratic regulator (LQR) was used. LQR's are controllers meant to regulate a certain state, bring its delta value to zero, while maintaining the closed loop response. Due to the nature of dynamic stability being built into the aircraft, meaning the states will naturally trend toward equilibrium, the LQR essentially prioritizes a certain state to stabilize over others. The general form for the controller of an LQR can be seen in Equation 17 where Q and R are user defined, weighted matrices that define the control system's response. A base relation can be made to help with guessing Q and R values, where a higher Q would result in the state moving to zero faster resulting in a larger control response and a higher R would be used to conserve control effect to stabilize the system, resulting in slower stabilizations.

$$J = \int_0^\infty \frac{1}{2}(\boldsymbol{x^T Q x} + \boldsymbol{u^T R u})\boldsymbol{dt} \tag{17}$$

A state-space for the aircraft cruising at Mach 0.9 at 40,000 feet was created using the linear dynamical models for both longitudinal and lateral motion created in section 3. Q and R values were defined in a separate MATLAB script that used the lqr() function to generate the K matrix for the gain block that feeds back into the control system. To find appropriate Q and R values, a guess-and-check strategy was used, mainly varying R and setting Q to the identity matrix. Figure 5 shows an example of the closed loop system, in this case, evaluating longitudinal motion of the aircraft. For each of the regulators, a set of initial conditions with small deflections was chosen and the Q and R values were adjusted to create a desired response. The initial conditions, the Q and R values, and the response of the particular state are listed for each section below in tables and Figures 6-17.

The current choices of Q and R are rough estimates that still require more fine tuning. While most produced reasonable responses, all can be improved and some require further analysis to confirm whether they are acceptable for final values. Section 4.1 has proven to be particularly tricky for finding appropriate values, more is discussed in section to improve the state the values are in.

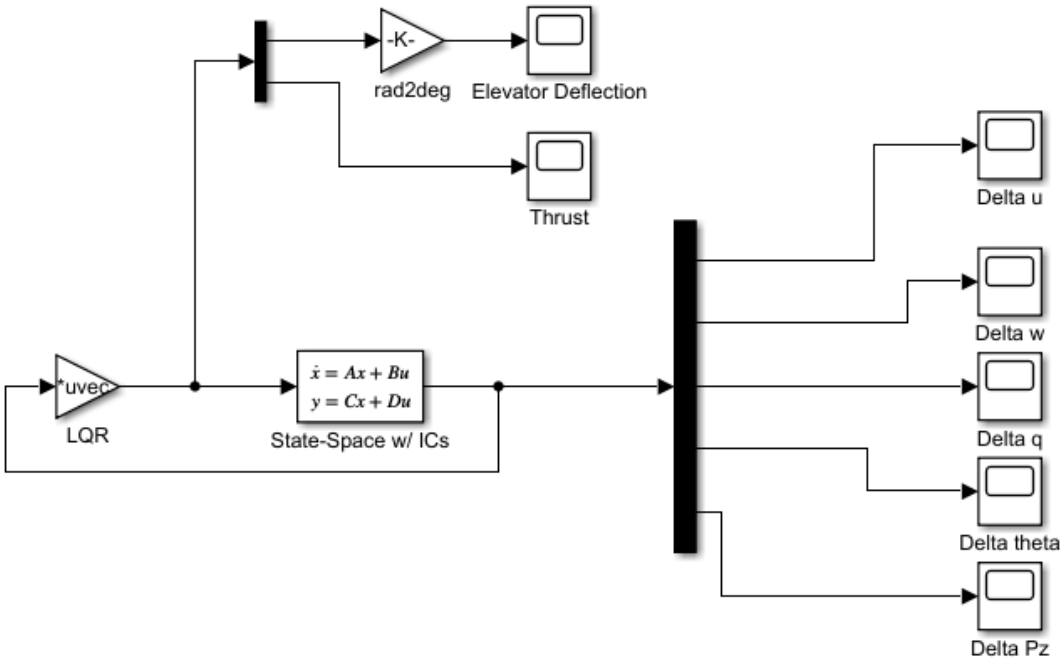

Figure 5: Simulink Model for the Regulation of Longitudinal Motion

4.1 Airspeed and Altitude Regulation

Initial Conditions	Q Matrix	R

$[10\ 0\ 0\ 0\ 0\ 10]$	$\begin{bmatrix} 1 & 0 & 0 & 0 & 0 \\ 0 & 1 & 0 & 0 & 0 \\ 0 & 0 & 1 & 0 & 0 \\ 0 & 0 & 0 & 1 & 0 \\ 0 & 0 & 0 & 0 & 1 \end{bmatrix}$	$\begin{bmatrix} 1000 & 0 \\ 0 & .003 \end{bmatrix}$

The initial conditions and Q and R values produced a fairly slow stabilization compared to the other regulators, ending up taking around 50 seconds to be within an acceptable margin away from equilibrium. This was mostly due to a large response required from the elevator deflection that could not be attainable for faster stabilization. Even with the slow stabilization, the maximum value of the elevator deflection was close to the maximum allowable deflection angle. The plots below show, as a function of time, the change in airspeed, altitude, elevator deflection and thrust.

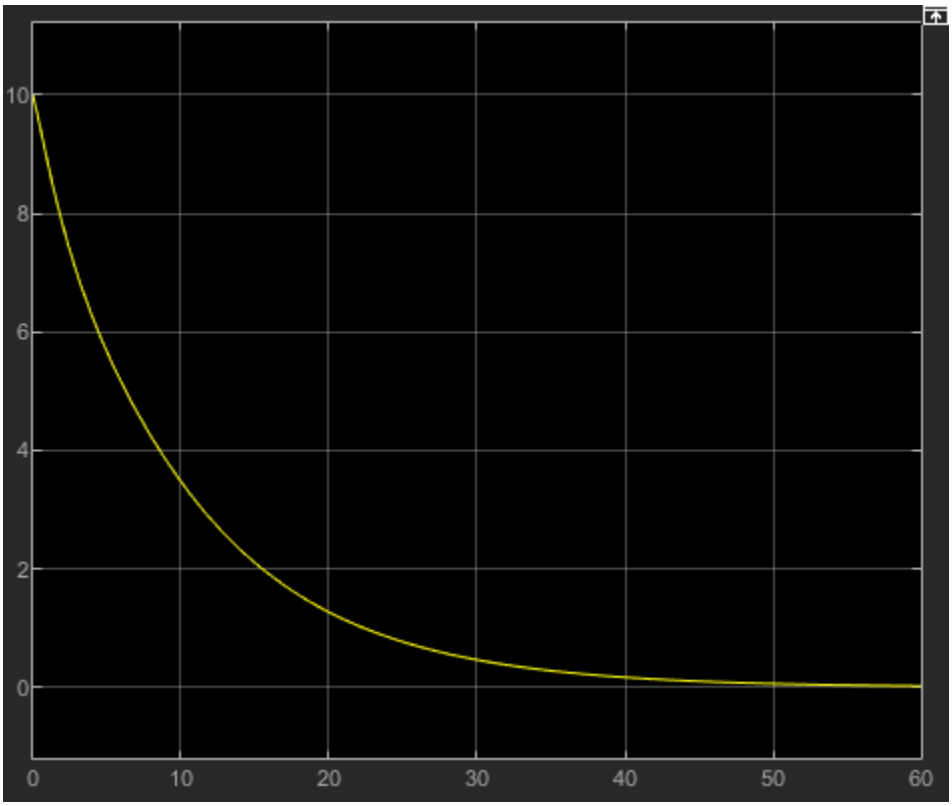

Figure 6: Simulink Scope of Airspeed Response (m/s)

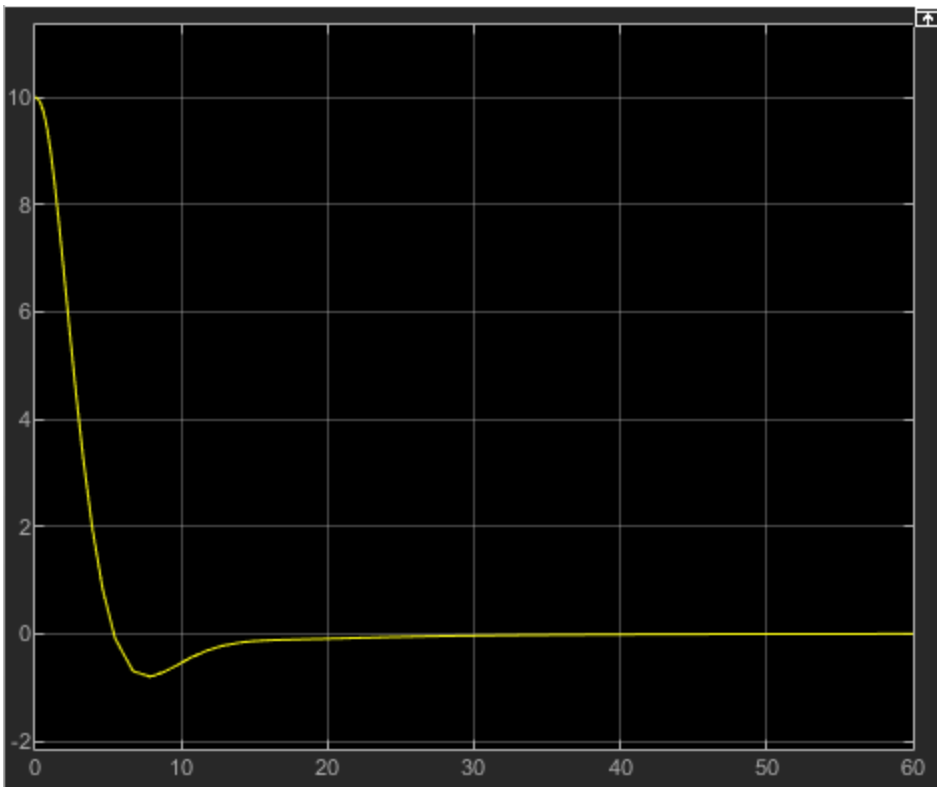

Figure 7: Simulink Scope of Altitude Response

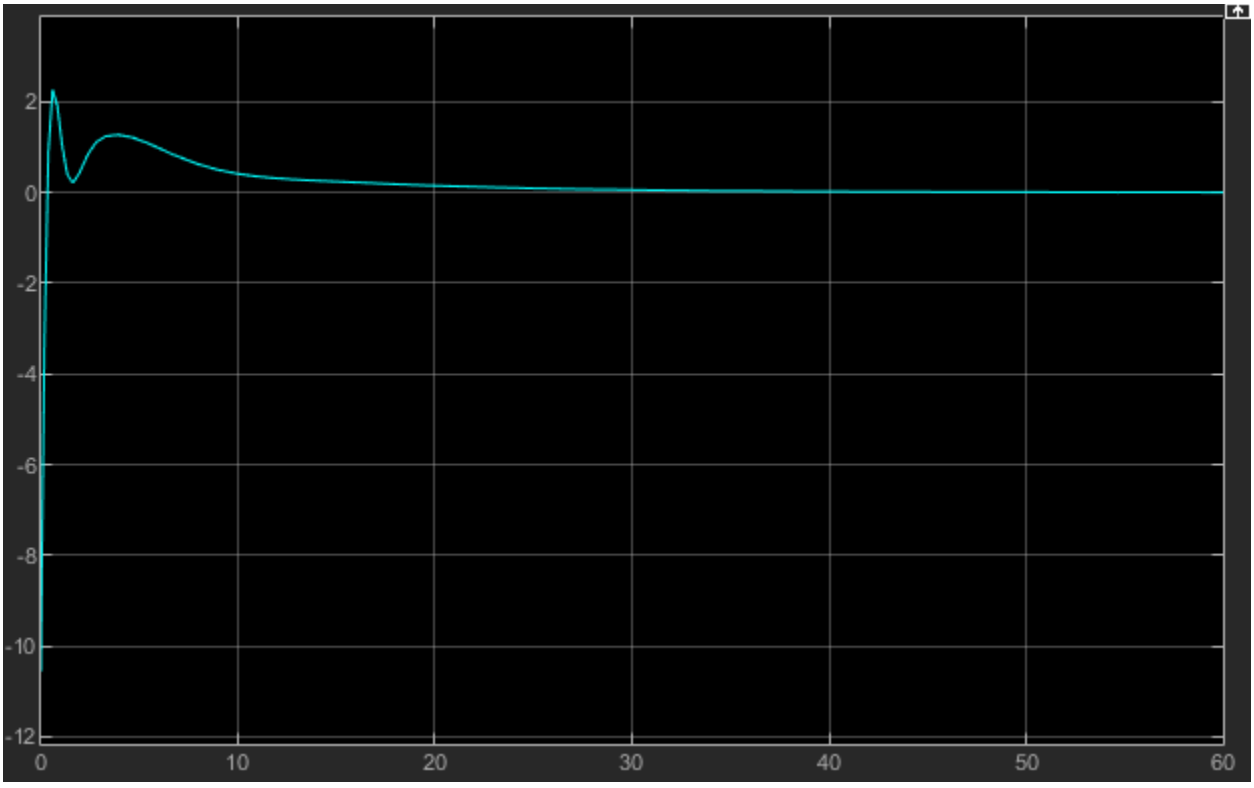

Figure 8: Simulink Scope of Aileron Deflection (deg)

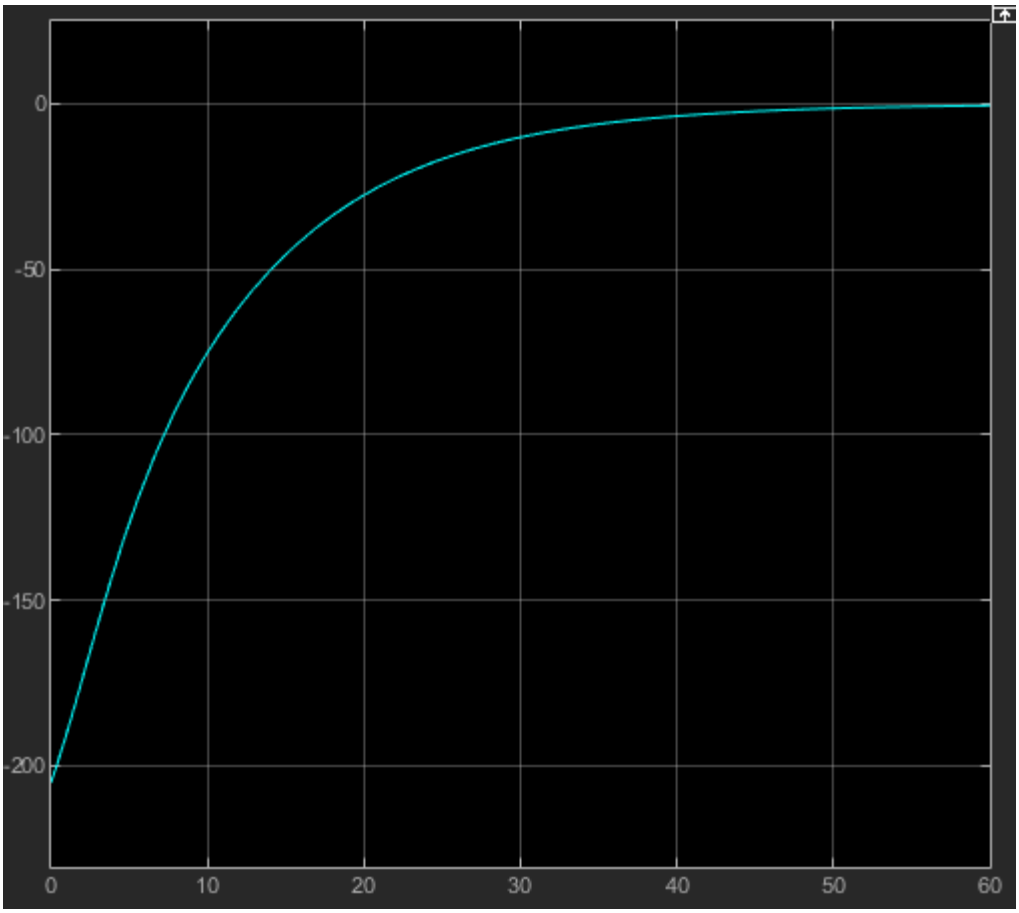

Figure 9: Simulink Scope of Change in Propulsion (N)

4.2 Pitch Regulation

Initial Conditions	Q Matrix	R
[0 0 0 0 3° 0]	$\begin{bmatrix} .01 & 0 & 0 & 0 & 0 \\ 0 & .01 & 0 & 0 & 0 \\ 0 & 0 & .01 & 0 & 0 \\ 0 & 0 & 0 & .01 & 0 \\ 0 & 0 & 0 & 0 & .01 \end{bmatrix}$	$\begin{bmatrix} 1000 & 0 \\ 0 & .003 \end{bmatrix}$

The initial conditions and Q and R values of this system produced a reasonable and quick regulation that has elevator deflection that is within realistic values. Settling time occurs within approximately 10 seconds, however an interesting observation from the response is that the pitch moves slightly away from equilibrium after 10 seconds and takes a while to go back towards it, however, not far enough to warrant it outside of an acceptable margin for being stable. The plots below show, as a function of time, the change in pitch, elevator deflection and thrust.

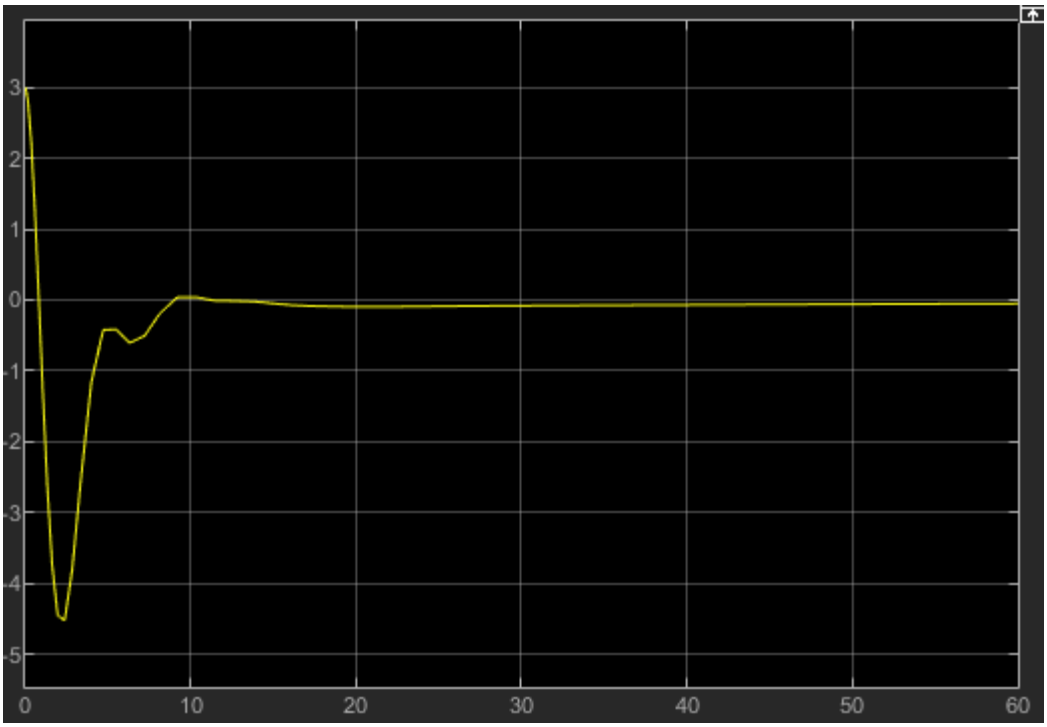

Figure 10: Simulink Scope of Pitch Response

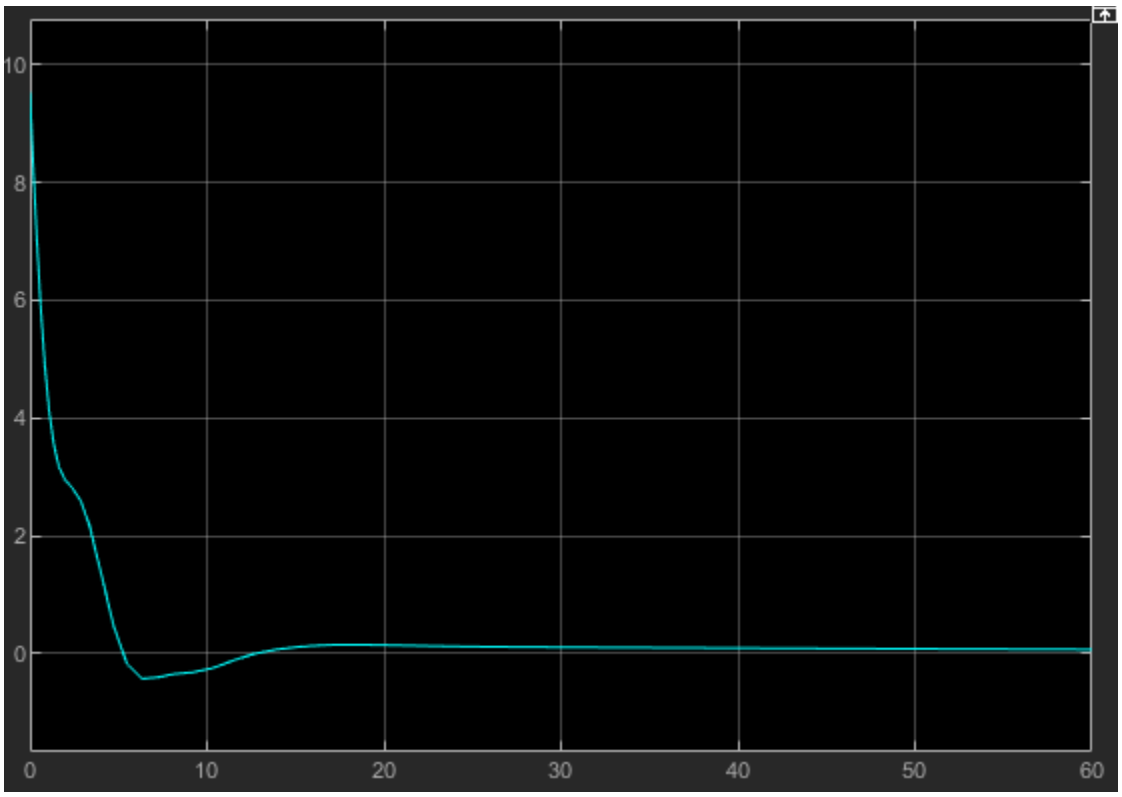

Figure 11: Simulink Scope of Aileron Deflection (deg)

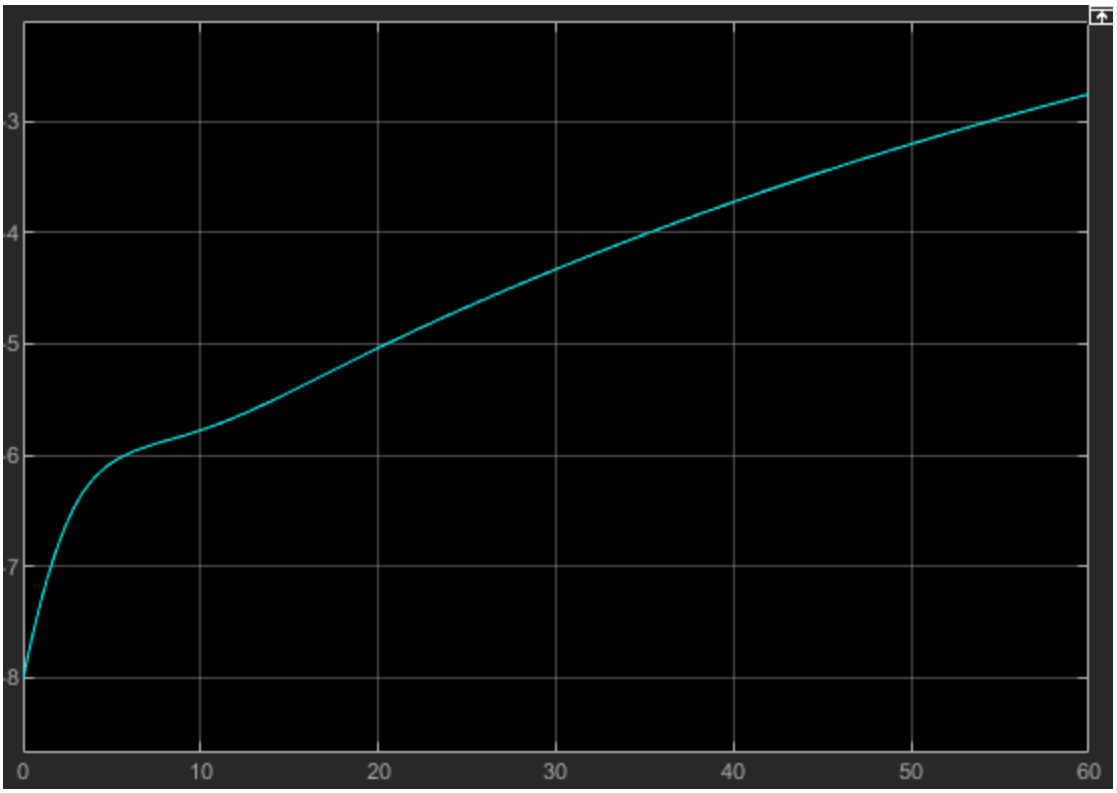

Figure 12: Simulink Scope of Change in Propulsion (N)

4.3 Roll Angle Regulation

Initial Conditions	Q Matrix	R
[0 0 0 0.0872 0 0]	$\begin{bmatrix} 1 & 0 & 0 & 0 & 0 & 0 \\ 0 & 1 & 0 & 0 & 0 & 0 \\ 0 & 0 & 1 & 0 & 0 & 0 \\ 0 & 0 & 0 & 1 & 0 & 0 \\ 0 & 0 & 0 & 0 & 1 & 0 \\ 0 & 0 & 0 & 0 & 0 & 1 \end{bmatrix}$	$\begin{bmatrix} 500 & 0 \\ 0 & 500 \end{bmatrix}$

The response to an initial roll angle error with these parameters settled in approximately 20 seconds, with a lightly damped response. Both aileron and rudder deflection remain within an acceptable range.

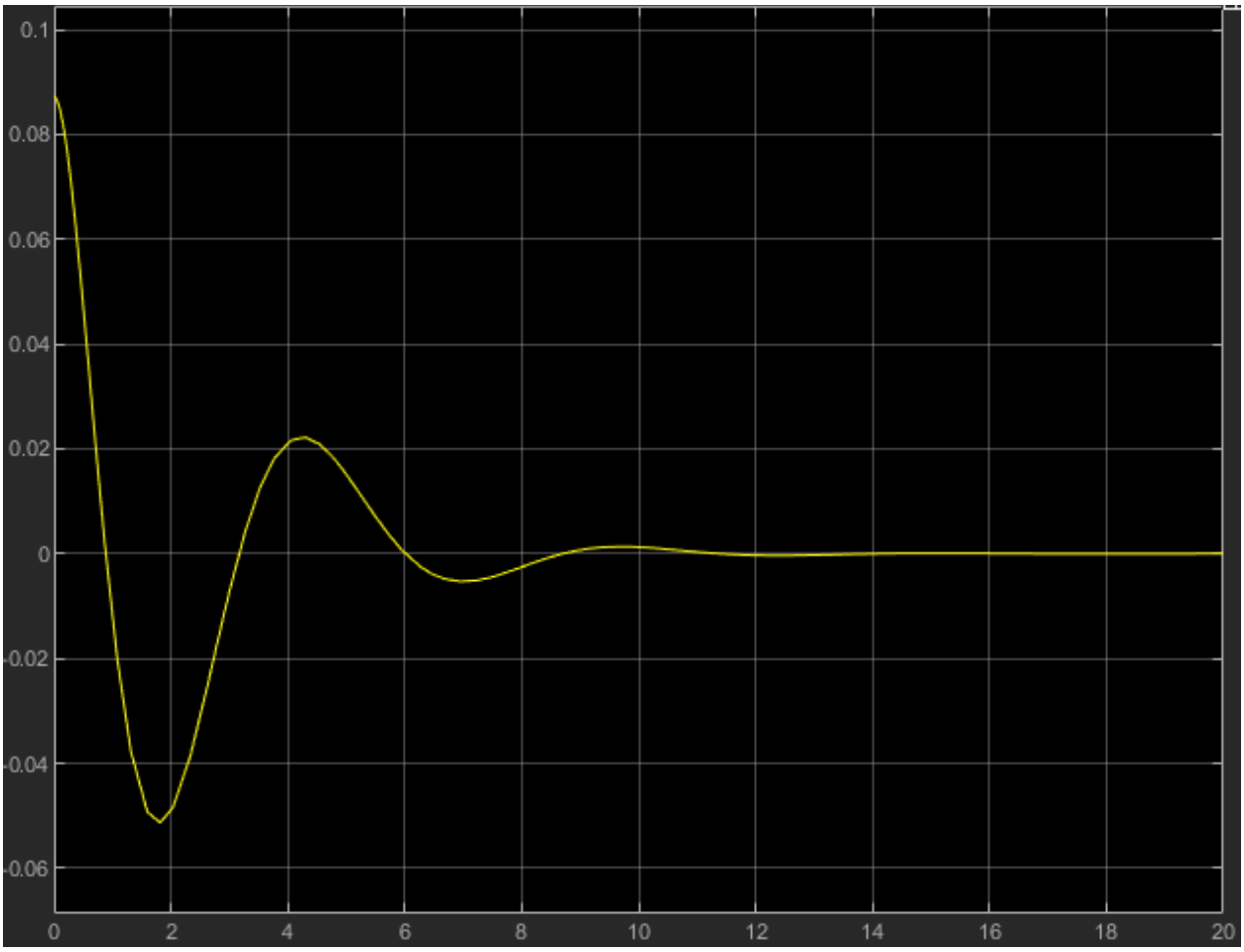

Figure 13: Simulink Scope of the Roll Response

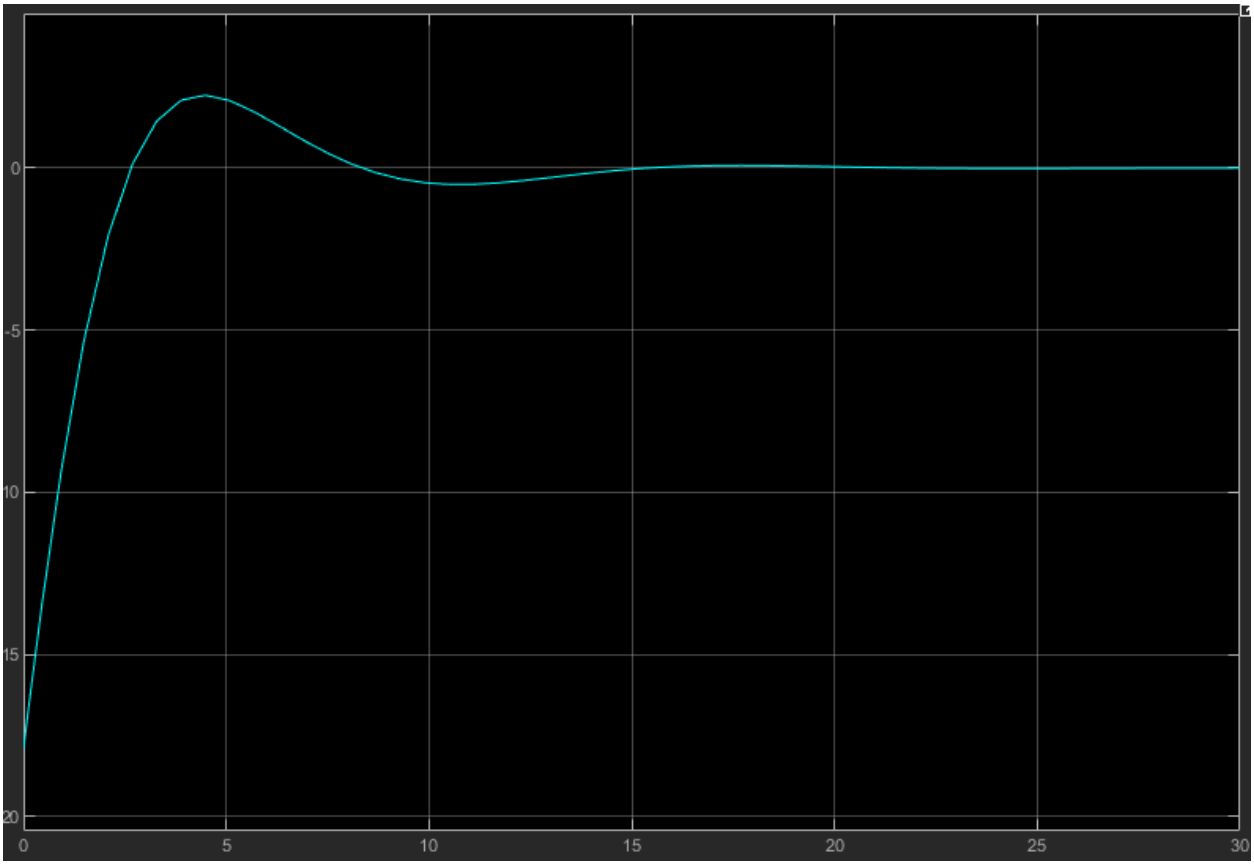

Figure 14: Simulink Scope of Aileron Deflection (deg)

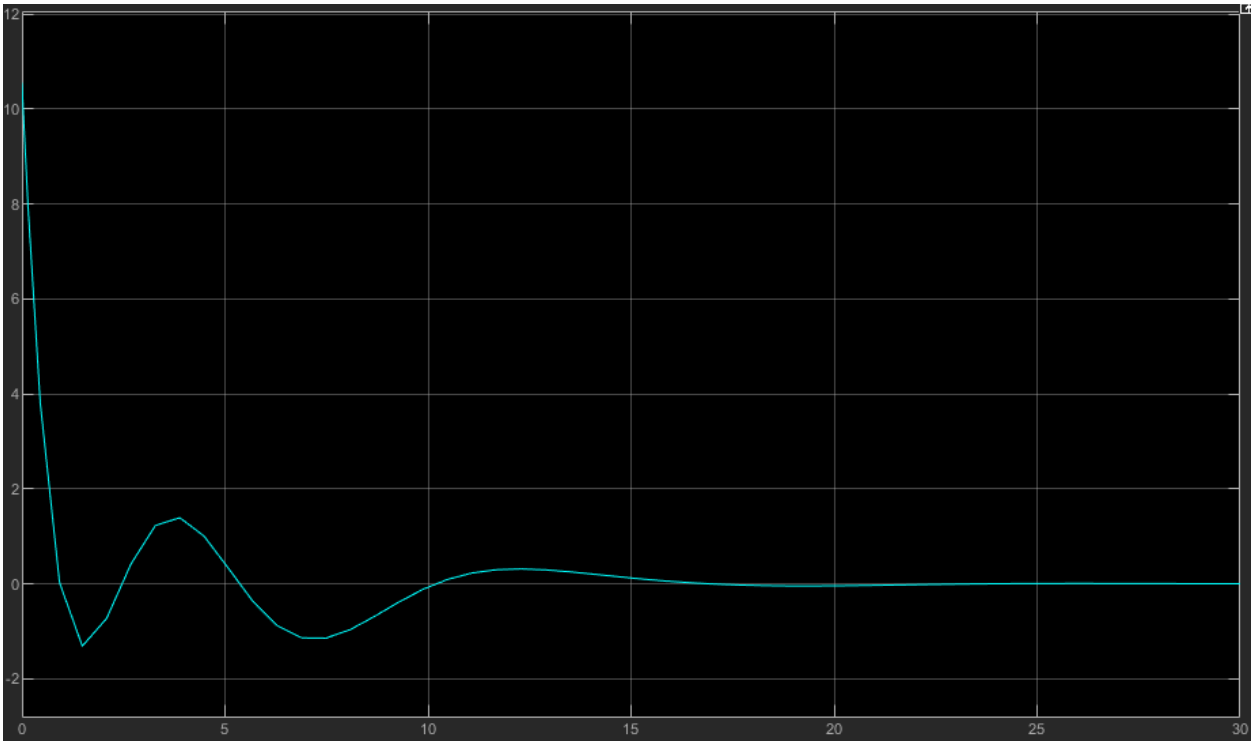

Figure 15: Simulink Scope of Rudder Deflection (deg)

4.4 Yaw Angle and Sideslip Regulation

Initial Conditions	Q Matrix	R
[0 0.5 0 0 0.0872 0]	$\begin{bmatrix} 0.02 & 0 & 0 & 0 & 0 & 0 \\ 0 & 0.02 & 0 & 0 & 0 & 0 \\ 0 & 0 & 0.02 & 0 & 0 & 0 \\ 0 & 0 & 0 & 0.02 & 0 & 0 \\ 0 & 0 & 0 & 0 & 0.02 & 0 \\ 0 & 0 & 0 & 0 & 0 & 0.02 \end{bmatrix}$	$\begin{bmatrix} 500 & 0 \\ 0 & 1000 \end{bmatrix}$

To simulate a sideslip, an initial condition of y velocity was included. Both the sideways velocity and yaw deflection settled in approximately one minute with a sizable overshoot in both cases with strong oscillatory motion. The yaw response produced an interesting motion, likely due to the system attempting to correct other states in the first 1.5 seconds, with the yaw angle returning to a value greater than the initial condition. In order create a tuning that would provide an acceptable response, but still yield acceptable aileron and rudder deflections, the settling time was extended.

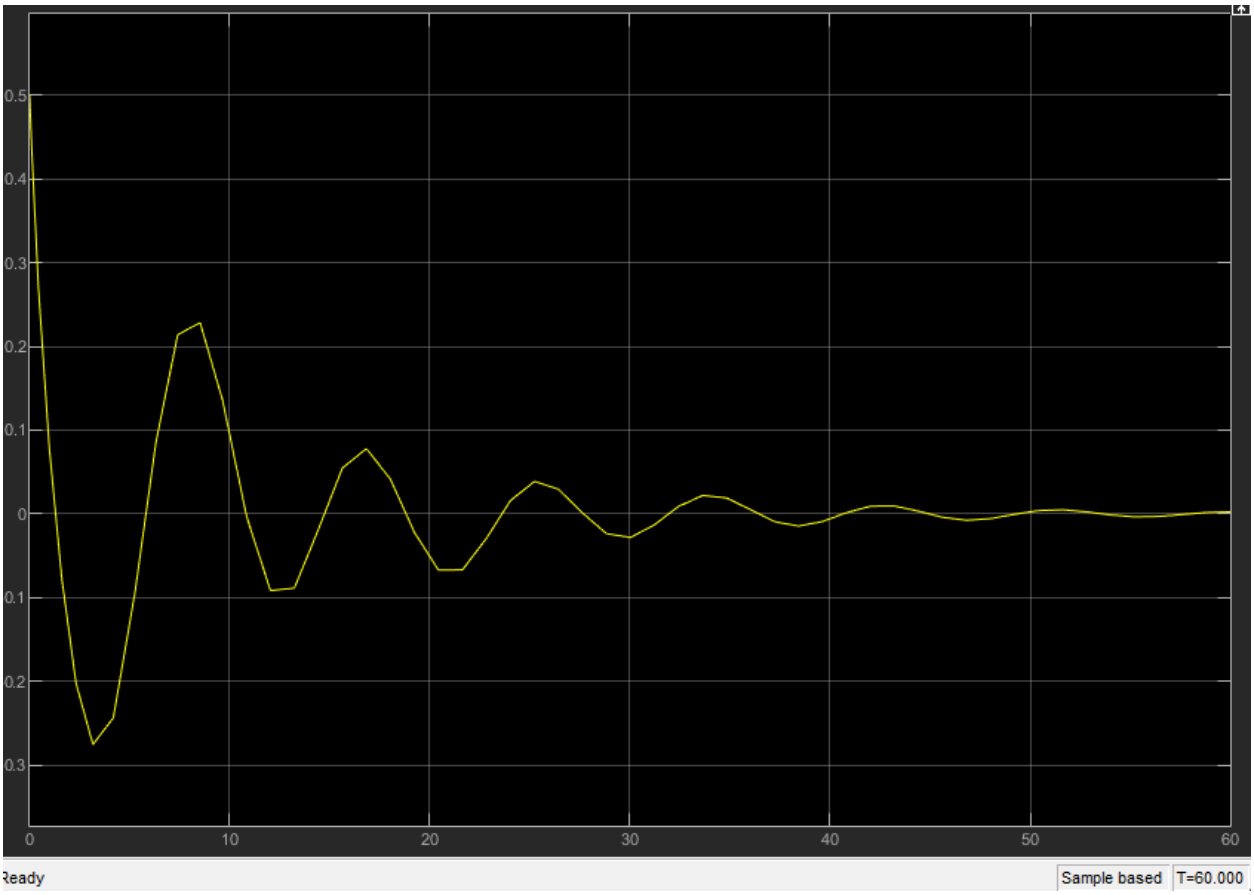

Figure 16: Simulink Scope of the y Axis Velocity (sideslip)

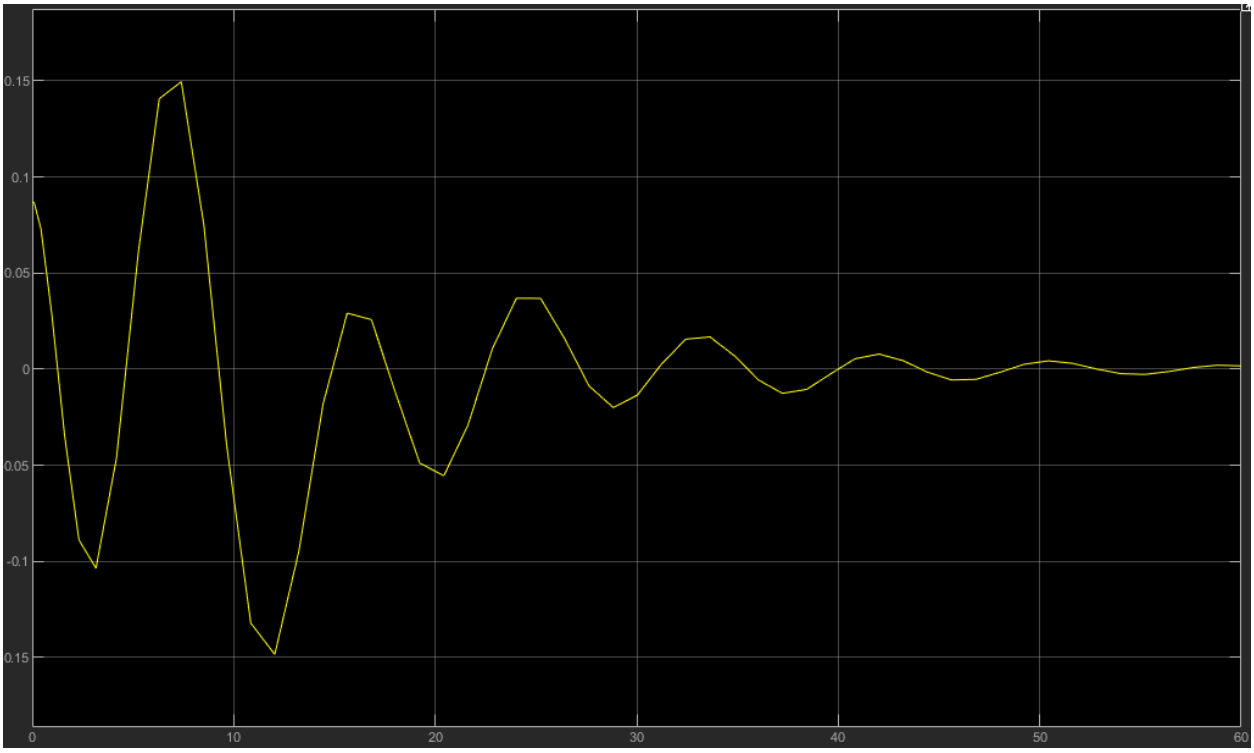

Figure 17: Simulink Scope of the Yaw Response

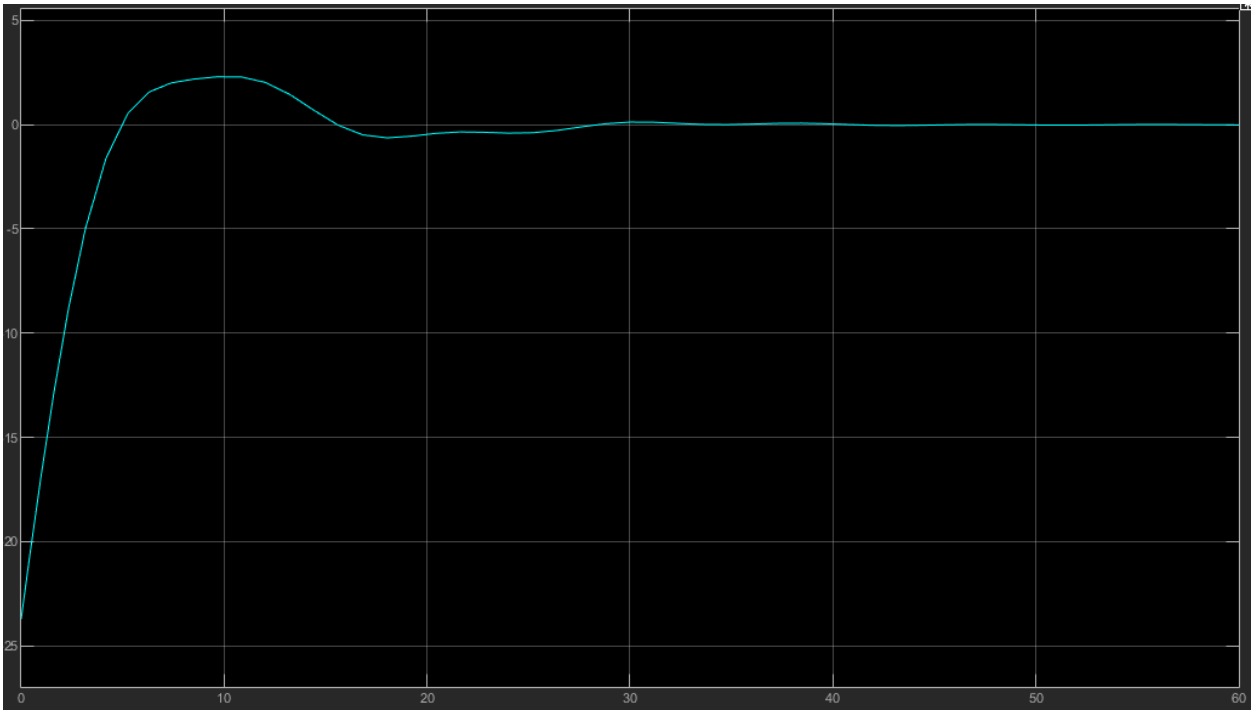

Figure 14 18: Simulink Scope of Aileron Deflection (deg)

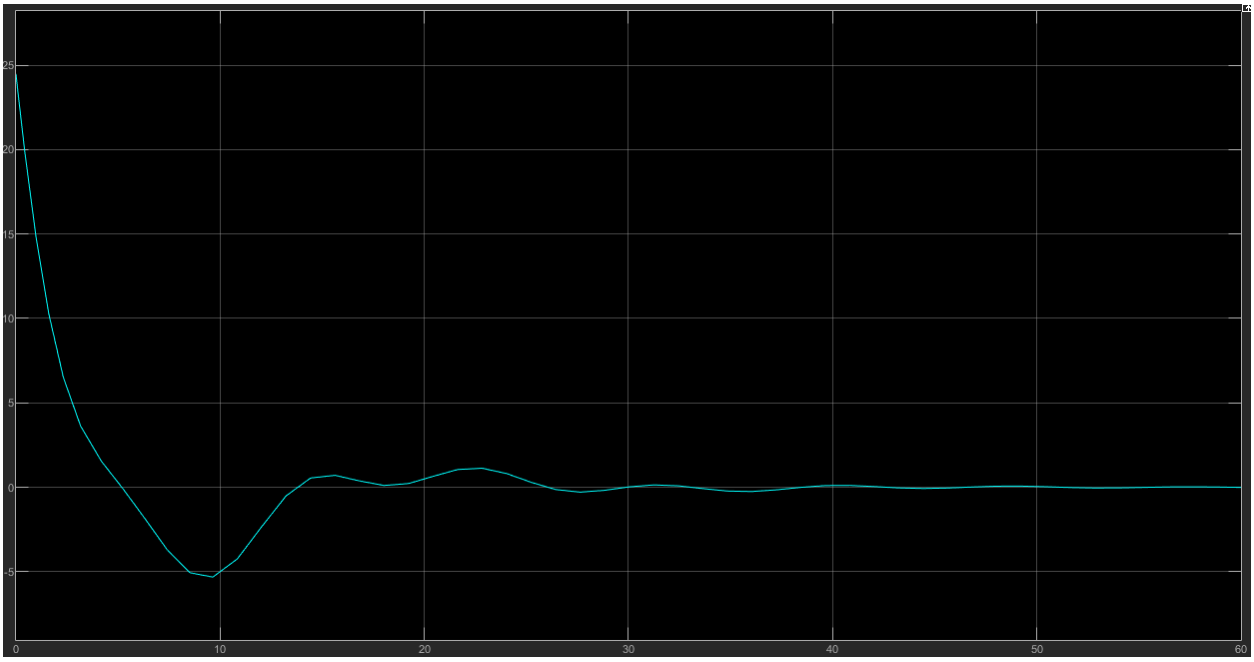

Figure 15 19: Simulink Scope of Rudder Deflection (deg)

5 Advanced Analysis

5.1 XFLR5 Airfoil Analysis

$Cl_{max,w}$ @ α = 21.5 deg	2.1
$Cl_{0,w}$	0.2
$Cl_{,w,\alpha}$	6.11
$Cl_{max,t}$ @ α = 24 deg	2.22
$Cl_{0,t}$	0
$Cl_{t,\alpha}$	6.366

A simple analysis was conducted within XFLR5 to determine and confirm critical aerodynamic parameters for the Boeing 747. First, to define an analysis, a working condition had to be set forth, which in this case was decided by the Reynolds number. As is known, a flow with equivalent Reynolds number can be modeled as an analysis in different conditions, which is particularly useful for modeling in situations where flows cannot be presumed to be incompressible in air. Calculations show that the Reynolds number for a 747 with an average chord of 9.27 meters, at a cruise speed of 0.816 Mach, and flying at an altitude of 6 km is around 100,000,000. Using the BACXXX airfoil from airfoiltools.com, the wing was analyzed first at the mean chord, from 0 to 25 degrees angle of attack. This Range allows for full development of the lift coefficient vs angle of attack curve. It is important to reach the stall point (in terms of

angle of attack) to determine the value of the maximum coefficient of lift. Yielding from this, the above parameters were deduced from graphical data when running in XFLR5. The same analysis was done for the NACA 4412 airfoil, adjusted to be symmetric, to act as the tail airfoil. These parameters served to find fairly accurate approximations for tail and wing aerodynamic coefficients, which were needed for analysis of alpha and elevator deflection at trim. The relationship between the angle of attack and the lift coefficient was deduced from the slope of the graph of Cl vs a. A similar method was used for the tail, evaluating from 0 to 25 degrees angle of attack, and extrapolating data graphically from XFLR5. The tail coefficient of lift is shown above as well.

The above parameters are critical to the stability analysis of the aircraft, as they help with determining the location of the neutral point and define the characteristics of the elevator deflection and angle of attack to attain specified trim conditions using control derivatives.

5.2 Flight Gear Simulation and Control Replication

5.2.1 Control Replication

Flight Gear was used to simulate different disturbance situations and visualize the dynamics of aircraft movement. Being that Flight Gear is a full-blown flight simulator meant for accurate flight training, with the physics of a given aircraft being replicated in the simulation. Calculation of control derivatives is applied in a similar fashion to Section 2 of this report. These control derivatives are given by Flight Gear, and the dynamics of the aircraft are modeled based on those same control derivatives. For this reason, the A and B matrices calculated for the B747 at the beginning of the project can be applied to testing the validity of simulations within Flight Gear. The aircraft used was a JBSIM designed Boeing 747-200 aircraft, with auto-pilot and simple keyboard user controls enabled. Setting the aircraft at a given trim condition was done using the auto-pilot feature and disturbances were made by setting the autopilot to different specifications. The three areas of possible analysis within the autopilot were relative altitude, air speed, and heading angle control. Shown below in Figure 12 is the aircraft at a trim, which is at altitude 40,000 ft., airspeed of 0.9 Mach or 580 knots, and heading angle of 200 degrees.

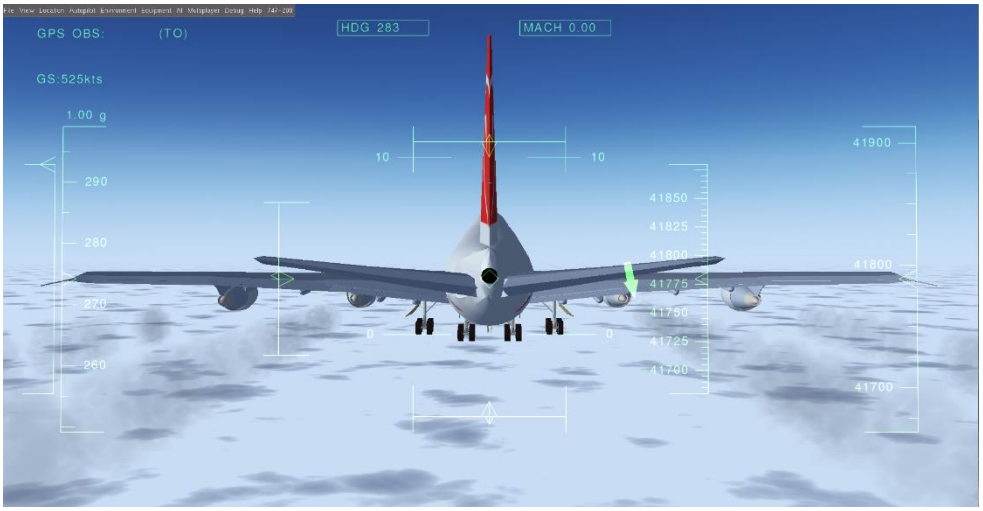

Figure 20: Boeing 747 Model in Flight Gear at trim conditions with autopilot enabled

Due to the complicated nature of collecting direct data from the Flight Gear software, it was decided that the following testing and confirmation method would be used to simulate our work:

1) Set the aircraft to offset (error) trim conditions in the flight simulator using the autopilot function.
2) Once the plane is settled at that trim, reset the trim to be the desired trim, one value at a time, repeating these steps for each of the following:
    a. Altitude
3) Manually time the settling of the aircraft to the "new" trim value, use the HUD display in flight gear to observe when oscillation stops so you can estimate time.
4) Using Simulink or other similar software, for EACH of the parameter errors listed in step 2, create a control loop with an lqr controller incorporating the A and B matrices specific to the aircraft
5) Reverse engineer the settling times found for each given disturbance by tuning the PID gains to the observed settling time from the Flight Gear software

Target Altitude (ft)	40,000 feet
Disturbance (ft)	500 feet
Settling Time (s)	95 seconds

An LQR controller was designed to try and replicate the 500 ft disturbance response seen in the Flight Gear simulation. The flight gear simulation runs off of a PID controller, but for simplicity, it was decided that the LQR controller would be used for altitude control. A simple closed-loop control system, with gain matrix K_long defined by control matrices R_long and Q_long, defined above, and found by guess and check methods, is used below in Simulink. The state-space model defines A, B, C, and D matrices as noted for longitudinal aircraft motion in Section 3. The fifth state in this linearized model is the change in altitude, which is aimed to be controlled when the disturbance of 500 feet is set as an initial condition.

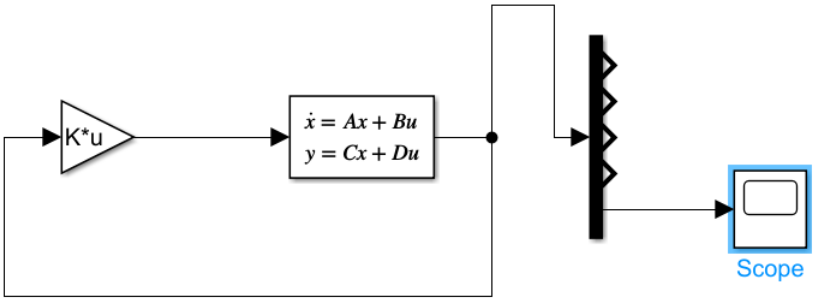

Figure 21: Simple control loop for modelling Altitude

Using guess and check methods, the LQR gain matrix was aiming to have a settling time of 95 seconds, which is the settling time observed for the trim condition in the previous table at 580 knots and 40,000 ft. For safe aircraft operation and comfort of passengers, a less aggressive response is desired. The plane in this case drops (controlled) by 100 meters in about ten seconds, this is characteristic of the response in flight gear, but is a bit of a steeper approach, but of course, not using a PID controller, it is difficult to directly emulate the response from the Flight Gear Simulation. At t = 10 seconds, the aircraft goes on a steady-time-rate glide path down to equilibrium at 40,000 ft or change in altitude is equal to zero on this graph. The settling time here is on the order of 100 seconds, which is very close to the 95 second settling time measured in Flight Gear. This difference can be attributed to the neglect of natural conditions in the linear model that has been set up in MATLAB. What this means is that Flight Gear simulates crosswinds and other conditions, while the linear model made in Simulink follows a purely x-direction flight with z-direction altitude change, and no sideslip.

This control method is generally favorable to service and absolute ceiling concerns, as it does not go above the target altitude, and does not create an extra disturbance (overshoot) in either direction. Both save on fuel and alleviate the risk of exaggeration of settling properties due to overshoot into the altitudes between the service and absolute ceilings, which is a real possibility given that this test was conducted at 40,500 ft initially.

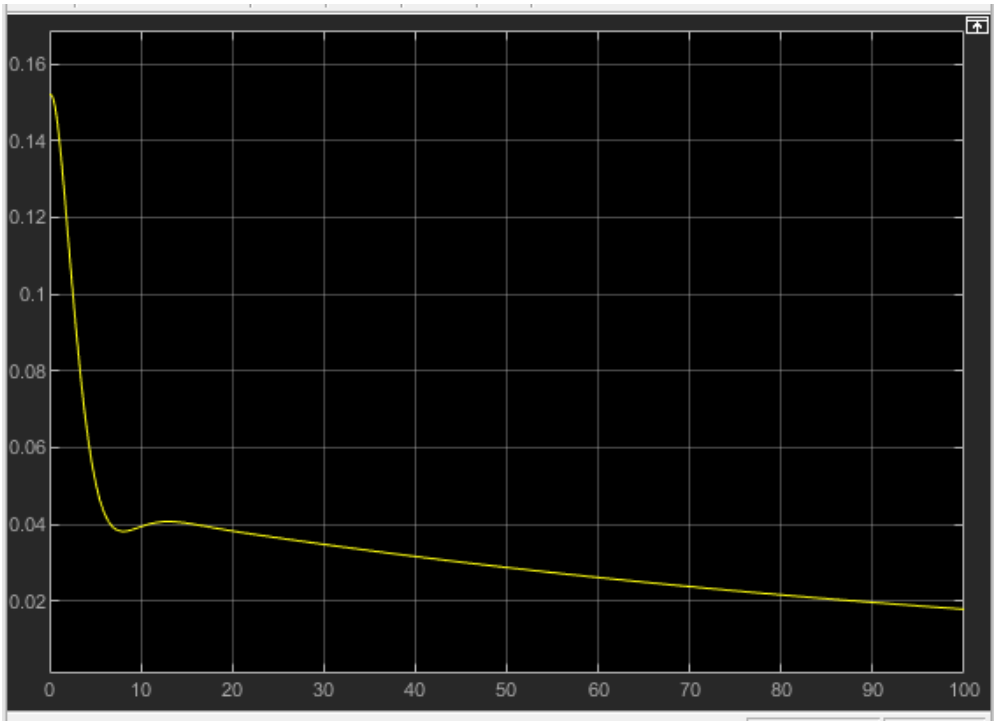

Figure 22: Reverse Engineered response for altitude control

Initial Conditions	Q Matrix	R
[0 0 0 0 0.152]	0.1*1 0 0 0 0 0 1 0 0 0 0 0 1 0 0 0 0 0 1 0 0 0 0 0 1	3.5

Tuned Gains for LQR controller mimicking Fight Gear PID

5.2.2 Stall and Ceiling Test

Instead of assuming that the dynamic model was accurate, a few tests were done to confirm different dynamical parameters. While the control loop reverse engineering serves as a technical visualization of how the control system may have been created, testing directly different dynamical parameters helps to gauge the accuracy of results. Absolute and service ceilings as well as the stall velocity will be confirmed in this section. Respectively, the absolute ceiling is 13.61 km, or 44,600 ft, the service ceiling is 13.39 km, or 43,000 ft, and the stall velocity is 108 m/s, or about 200 knots.

The first test performed in the simulator was the service ceiling. By placing the plane above the service ceiling using the “locate” command in Flight Gear, the properties of the plane in the area between the absolute and service ceilings could be observed. If erratic behavior is observed, it

would be safe to say that the aircraft would be in close range to the service and absolute ceilings, as the service ceiling defines erratic behavior, and the absolute ceiling indicated lack of climb capability. When placing the aircraft at the service ceiling of about 43,000 feet, autopilot was set to lift it to 44,000 to cruise at 580 knots. Placement here resulted in extreme oscillation of the aircraft which is shown as a forward and back pitching motion in Figure 13. The settling mode at that instant seems to be the phugoid mode, as the aircraft has a long lightly damped response in its return to stability. Observing this phenomenon at different altitudes also resulted in the same mode, but often with smaller pitch changed, which was much less aggressive.

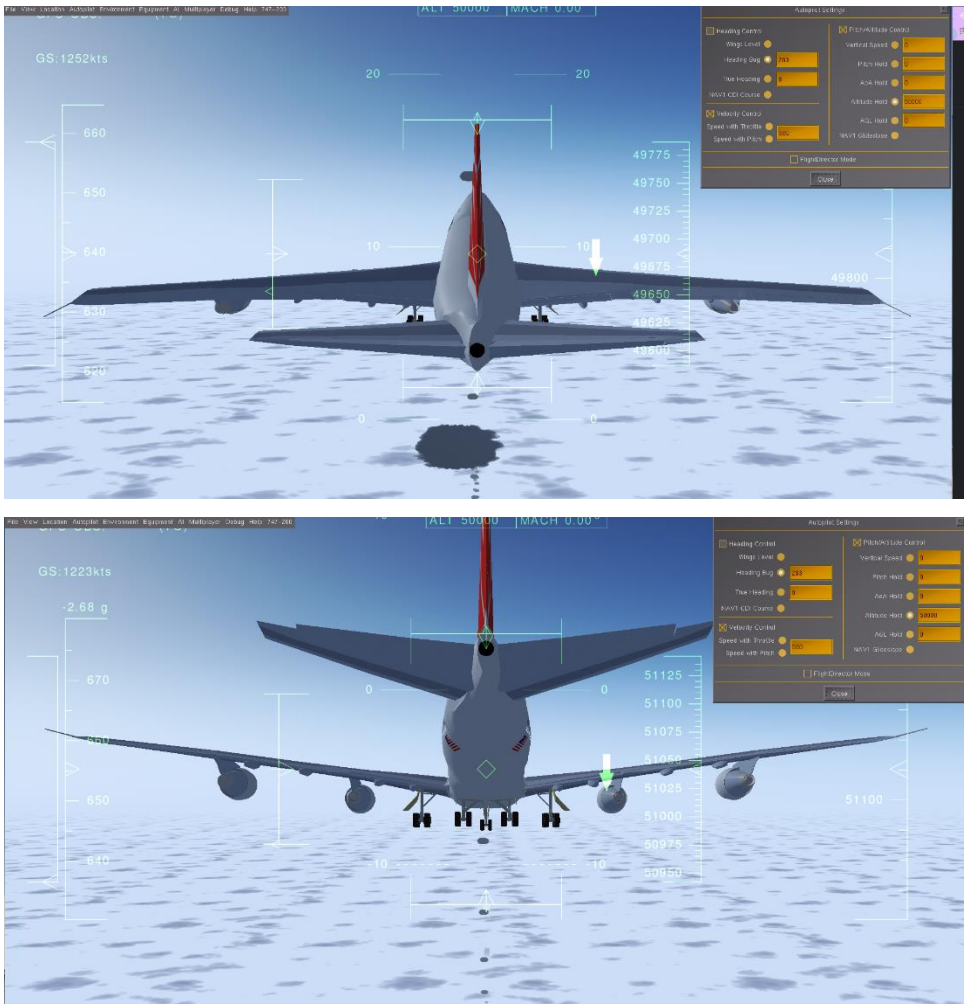

Figure 23: Examples of erratic pitching motion in between the absolute and service ceilings

Observing the absolute ceiling also proved to show accuracy in our previous calculations. When setting the aircraft above 44,600 ft, the aircraft would plunge downwards and violently oscillate. This is characteristic of the absolute ceiling, as it is the location where the aircraft can no longer climb, meaning when placed above that altitude, it must settle back to the absolute ceiling itself, as observed in Flight Gear.

The last parameter confirmed in Flight Gear is stall. Earlier in the project, stall was calculated to be 200 knots, or about 108 m/s. Setting the aircraft at this velocity in Flight Gear cause the aircraft to begin steady decent, as the aircraft could not linger produce enough thrust and lift to outweigh its own weight, as well as aerodynamic drag. The aircraft was set to a zero pitch, which characterizes the point that the stall velocity was originally calculated for at 20,000 ft. Figure 14 shows the steady fall of the aircraft at 200 knots as it was unable to climb any further. This is further confirmed by the autopilot setting at 200 knots and 20,000 ft, as the 20,000 ft margin could not be met despite proper control design.

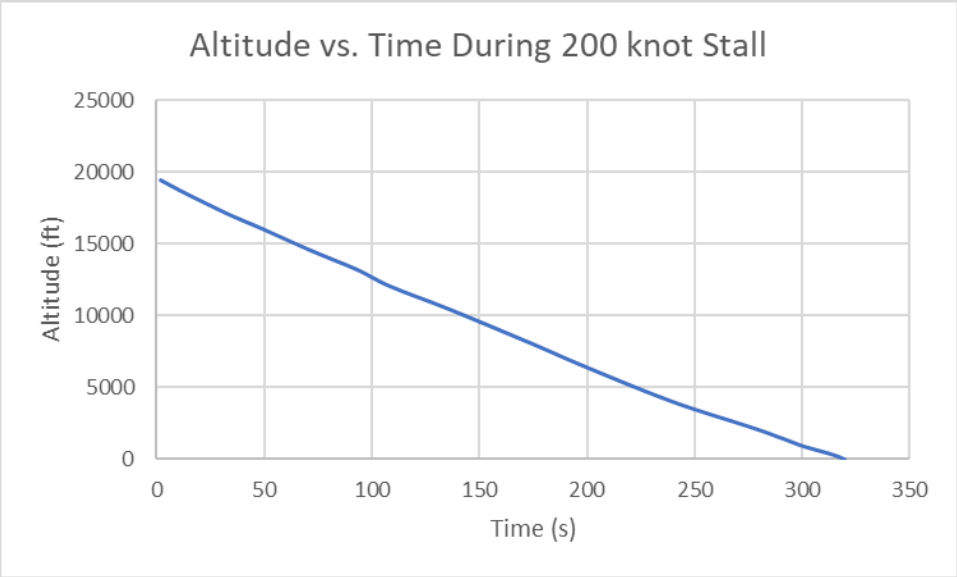

Figure 24: Altitude vs. Time graph for stall at V_{stall} from Section 1

6 References

Boeing 747-400. Airliners.net. (n.d.). Retrieved January 29, 2022, from https://www.airliners.net/aircraft-data/boeing-747-400/100

Boeing 747 8 Specs the newest Jumbo Jet Modern Airliners. (n.d.). Retrieved January 28, 2022, from https://modernairliners.com/boeing-747-8/boeing-747-8i-and-8f-specs/

Center of Gravity Limitations. Smart Cockpit. (n.d.). Retrieved February 4, 2022, from https://www.smartcockpit.com/aircraft-ressources/Center_Of_Gravity_Limitations.html

Koşar, K., Durmaz, S., & Jafarov, E. M. (2007). LONGITUDINAL DYNAMICS ANALYSIS of BOEING 747-400 . In *Proceedings of the 9th WSEAS International Conference on Automatic Control, Modeling & Simulation, Istanbul, Turkey*. Istanbul, Turkey; Istanbul Technical University Department of Aeronautics and Astronautics.

Nelson, R. C. (2010). Appendix. In *Flight stability and automatic control*. essay, WCB/McGraw-Hill Education.

Sun, J., Hoekstra, J. M., & Ellerbroek, J. (2018). *Aircraft Drag Polar Estimation Based on a Stochastic Hierarchical Model*. 8.

Virginia Tech Department of Aerospace and Ocean Engineering. (1993, March 17). *Boeing 747-400 Dynamic Analysis*. Blacksburg, VA.

What is the difference between absolute and service ceiling? | Essential Pilot. (n.d.). Retrieved January 28, 2022, from http://essentialpilot.co.za/2020/05/10/absolute-v-service-ceiling-in-the-climb-what-is-the-difference/

7 Appendix: Code Developed

The following script contains MATLAB code developed for the analysis of both lateral and longitudinal dynamics at multiple Mach numbers and altitudes.

```
clc; close all; clear all;
% For the different Altitudes and Mach numbers, the constants for the case
% being evaulated are uncommented, while leaving all others commented out.
% By default,Mach 0.25 at Sea level is selected

%Longitudinal, M = 0.25, Sea level
M = 0.25;
h = 0;
a1 = 6.5;
Tsl = 288.16;
T = Tsl - a1*h;
gamma = 1.4;
R = 286;
mach = sqrt(gamma*R*T);
V = M*mach;


Cl_ = 1.11;
Cd_ = 0.102;
Cl_a = 5.7;
Cd_a = 0.66;
Cm_a = -1.26;
Cl_adot = 6.7;
Cm_adot = -3.2;
Cl_q = 5.4;
Cm_q = -20.8;
Cl_de = 0.338;
Cm_de = -1.34;

%Lateral M = 0.25, Sea level
Cy_b = -0.96;
Cl_b = -0.221;
Cn_b = 0.150;
Cl_p = -0.45;
Cn_p = -0.121;
Cl_r = 0.101;
Cn_r = -0.3;
Cl_da = 0.0461;
Cn_da = 0.0064;
Cy_dr = 0.175;
Cl_dr = 0.007;
Cn_dr = -0.109;

% %Longitudinal, M = 0.90, 40,000ft
% M = 0.9;
% h = 12192/1000;
% Tsl = 288.16;
% a1 = 6.5;
% T = Tsl - a1*h;
```

```
% gamma = 1.4;
% R = 286;
% mach = sqrt(gamma*R*T);
% V = M*mach
%
% Cl_ = 0.5;
% Cd_ = 0.042;
% Cl_a = 5.5;
% Cd_a = 0.47;
% Cm_a = -1.6;
% Cl_adot = 0.006;
% Cm_adot = -9.0;
% Cl_q = 6.58;
% Cm_q = -25.0;
% Cl_de = 0.3;
% Cm_de = -1.2;
%
% %Lateral M = 0.9, 40,000 ft
%
% Cy_b = -0.85;
% Cl_b = -0.1;
% Cn_b = 0.2;
% Cl_p = -0.3;
% Cn_p = 0.2;
% Cl_r = 0.2;
% Cn_r = -0.325;
% Cl_da = 0.014;
% Cn_da = 0.003;
% Cy_dr = 0.075;
% Cl_dr = 0.005;
% Cn_dr = -0.09;

% % Longitudinal, V = 673 ft/s, 20,000 ft
% V = 673 ;
% h = 6.5
% a1 = 6.5;
%
% Cl_ = 0.4;
% Cd_ = 0.025;
% Cl_a = 4.4;
% Cd_a = 0.2;
% Cm_a = -1;
% Cl_adot = 7;
% Cm_adot = -4;
% Cl_q = 6.6;
% Cm_q = -20.5;
% Cl_de = 0.32;
% Cm_de = -1.3;

% Standard Atmospheric model to determine density:
p =1.225*(1-h*a1/288.16)^(-1-9.8/(-.0065*287));

%aircraft parameters
m = 362875;
b = 64.44;
c = 541.2/64.44;
```

```
S = 541.2;
g = 9.81;

%trim conditions, with further coefficients defined:
V_ = V;
u_ = V;
p_ = p;
theta_ = 0;
Ct_ = 1/(6200);
Cl_u =0;
Cd_u = 0;
Cm_u = 0;
Cd_de = 0;
Cy_p = 0;
Cy_r = 0;
Ct_u = 0;
Cm_dp = 0;
Cy_da = 0;

%%LONGITUDINAL MOTION%%

%Mass moments of inertia
Jx = 1.82*10^7*1.3558;
Jy = 3.31*10^7*1.3558;
Jz = 4.97*10^7*1.3558;
Jzx = 97*10^4*1.3588;
%dimensional derivatives
Xw = .5*p_*V_*S*(Cl_ - Cd_a);
Xu = 2*m*g*sind(theta_)/V_ -.5*p_*V_*S*(Cd_u + 2*Cd_);
Xq = 0;
X_wdot = 0;
Xde = -.5*p_*V_^2*S*Cd_de;
Xdp = .5*p_*V_^2*S*(Ct_u + 2*Ct_);

Zu = -2*m*g*cos(theta_)/(V_)-.5*p_*V_*S*(Cl_u + 2*Cl_);
Zw = -.5*p_*V_*S*(Cd_ + Cl_a);
Zw_dot = -.25*p_*S*c*Cl_adot;
Zq = -.25*p_*V_*S*c*Cl_q;
Zde = -.5*p_*V_*S*c*Cl_de;
Zdp = 0;

Mq = .25*p_*V_*S*c*Cm_q;
Mu = .5*p_*V_*S*c*Cm_u;
Mw = .5*p_*V_*S*c*Cm_a;
Mw_dot = 0.25*p_*S*c^2*Cm_adot;
Mde = .5*p_*V_^2*S*c*Cm_de;
Mdp = .5*p_*V_^2*S*c*Cm_dp;

%Longitudinal Matrices
M_p = Mw_dot/(m-Zw_dot)

A11 = Xu/m
A12 = Xw/m
A13 = 0
A14 = -g*cos(theta_)
```

```
A15 = 0

A21 = Zu/(m-Zw_dot)
A22 = Zw/(m-Zw_dot)
A23 = (Zq + m*u_)/(m-Zw_dot)
A24 = (-m*g*sin(theta_)/(m-Zw_dot))
A25 = 0

A31 = (Mu +M_p*Zu)/Jy
A32 = (Mw + M_p*Zw)/Jy
A33 = (Mq + M_p*(Zq + m*u_))/(Jy)
A34 = -M_p*m*g*sin(theta_)/Jy
A35 = 0

A51 = -sin(theta_)
A52 = cos(theta_)
A53 = 0
A54 = -u_*cos(theta_)
A55 = 0

B11 = Xde/m
B12 = Xdp/m

B21 = Zde/(m-Zw_dot)
B22 = Zdp/(m-Zw_dot)

B31 = Mde/Jy + Mw_dot*Zde/(Jy*(m-Zw_dot))
B32 = Mdp/Jy + Mw_dot*Zdp/(Jy*(m-Zw_dot))

B41 = 0
B42 = 0

B51 = 0
B52 = 0

A_long = [A11, A12, A13, A14, A15;
          A21, A22, A23, A24, A25;
          A31, A32, A33, A34, A35;
          0, 0, 1, 0, 0;
          A51, A52, A53, A54, A55]

B_long = [B11, B12;
          B21, B22;
          B31, B32;
          B41, B42;
          B51, B52]

% Defining Q and R values to determine LQR gain
Q_long = [1 0 0 0 0;
          0 1 0 0 0;
          0 0 1 0 0;
          0 0 0 1 0;
          0 0 0 0 1];
```

```
R_long = 5;

% Finding LQR gain based on A,B,Q,and R
K_long = lqr(A_long, B_long, Q_long, R_long, zeros(5,2))

% Finding Eigenvalues to determine modes and settling times

eig2 = eig(A_long)

% Seperating real compoments and finding settling time of each mode
E = real(eig2)
ts = 4/(-E(1))
ts = 4/(-E(2))
ts = 4/(-E(3))
ts = 4/(-E(4))
ts = 4/(-E(5))

% Determining damping ratios with a vpa solver based on the real components
% of the eigenvalues:
dlo=[0];
syms dam
for i=1:1:5
    i;
wn=-E(i)/dam;
eqn=wn*sqrt(1-dam^2);
eqns=subs(eqn);
dlo(i)=vpa(solve(eqns==imag(eig2(i)),dam));
end
dlo

%%LATERAL MOTION%%

% Defining dimensional derivatives for lateral motion
lv = 0.5*p_*V_*S*b*Cl_b;
lr = 0.25*p_*V_*S*b^2*Cl_r;
lp = 0.25*p_*V_*S*b^2*Cl_p;

lda = 0.5*p_*V_^2*S*b*Cl_da;
ldr = 0.5*p_*V_^2*S*b*Cl_dr;

Nv = 0.5*p_*V_*S*b*Cn_b;
Nr = 0.25*V_*p_*S*b^2*Cn_r;
Np = 0.25*p_*V_*S*b^2*Cn_p;

Nda = 0.5*p_*V_^2*S*b*Cn_da;
Ndr = 0.5*p_*V_^2*S*b*Cn_dr;

Yda = 0.5*p_*V_^2*S*Cy_da;
Ydr = .5*p_*V_^2*S*Cy_dr;

Yp = .25*p_*V_*S*b*Cy_p;
Yr = 0.25*p_*V_*S*b*Cy_r;
Yv = .5*p_*V_*S*Cy_b;
```

```
Jp_zx = Jzx/((Jx*Jz - Jzx^2));
Jp_x = (Jx*Jz - Jzx^2)/Jz;
Jp_z = (Jx*Jz - Jzx^2)/Jx;

%Lateral A matrix
A_11 = Yv/m;
A_12 = Yp/m ;
A_13 = -V_ + Yr/m;
A_14 = g*cos(theta_);
A_15 = 0;
A_16 = 0;

A_21 = lv/(Jp_x)+Jp_zx*Nv;
A_22 = lp/(Jp_x)+Jp_zx*Np;
A_23 = lr/(Jp_x)+Jp_zx*Nr;
A_24 = 0;
A_25 = 0;
A_26 = 0;

A_31 = Nv/(Jp_z)+Jp_zx*lv;
A_32 = Np/(Jp_z)+Jp_zx*lp;
A_33 = Nr/(Jp_z)+Jp_zx*lr;
A_34 = 0;
A_35 = 0;
A_36 = 0;

A_41 = 0;
A_42 = 1;
A_43 = tan(theta_);
A_44 = 0;
A_45 = 0;
A_46 = 0;

A_51 = 0;
A_52 = 0;
A_53 = sec(theta_);
A_54 = 0;
A_55 = 0;
A_56 = 0;

A_61 = 1;
A_62 = 0;
A_63 = 0;
A_64 = 0
A_65 = V_*cos(theta_);
A_66 = 0;

%Lateral B matrix
B_11 = Yda/m
B_12 = Ydr/m

B_21 = lda/(Jp_x)+Jp_zx*Nda
B_22 = ldr/(Jp_x)+Jp_zx*Ndr

B_31 = Nda/(Jp_z)+Jp_zx*lda
```

```
B_32 = Ndr/(Jp_z)+Jp_zx*ldr

B_41 = 0
B_42 = 0

B_51 = 0
B_52 = 0

B_61 = 0
B_62 = 0

A_lat = [A_11, A_12, A_13, A_14, A_15, A_16;
    A_21, A_22, A_23, A_24, A_25, A_26;
    A_31, A_32, A_33, A_34, A_35, A_36;
    A_41, A_42, A_43, A_44, A_45, A_46;
    A_51, A_52, A_53, A_54, A_55, A_56;
    A_61, A_62, A_63, A_64, A_65, A_66]

B_lat =  [B_11, B_12;
          B_21, B_22;
          B_31, B_32;
          B_41, B_42;
          B_51, B_52;
          B_61, B_62]
% Defining Q and R values to determine LQR gain
Q_lat = eye(6)
R_lat = 5;

% Finding LQR gain based on A,B,Q,and R
K_lat = lqr(A_lat, B_lat, Q_lat, R_lat, zeros(6,2))

eig2 = eig(A_lat)

% Seperating real compoments and finding settling time of each mode
E = real(eig2)
ts = 4/(-E(1))
ts = 4/(-E(2))
ts = 4/(-E(3))
ts = 4/(-E(4))
ts = 4/(-E(5))
ts = 4/(-E(6))

% Determining damping ratios with a vpa solver based on the real components
% of the eigenvalues:
dlo=[0];
syms dam
for i=1:1:6
    i;
wn=-E(i)/dam;
eqn=wn*sqrt(1-dam^2);
eqns=subs(eqn);
vpa(solve(eqns==imag(eig2(i)),dam))
end
```